POLITECNICO DI TORINO

Master degree course in Biomedical Engineering

Master Degree Thesis

High density EMG signal decomposition for force prediction: perspective for man-machine interfacing

Supervisor
Prof. Marco Gazzoni

Co-supervisor
Prof. Dario Farina

Candidate
Marianna Felizzi

Academic Year 2018-2019

Abstract

The surface electromyogram (EMG) is used to infer the neural drive sent by the central nervous system to the muscles by associating its amplitude to the strength of the neural activation. In addition, the surface EMG is adopted in the design of technologies for motor rehabilitation with the aim to restore the lost limb functionality of amputees. In this perspective, it is possible to translate this biologic signal into commands for controlling intuitively the prosthetic device.

Since the surface EMG amplitude constitutes a poor indicator of the neural information, more advanced methods were developed such as the high-density surface EMG signal decomposition. With this work, I focused my efforts on understanding how the central nervous system (CNS) controls the muscle force, by exploiting the discharge timings of the motor units. This might help to lay the foundations for an innovative human-machine interface directly based on the spinal cord circuitry information. In this context, the aim of this thesis is to compare the use of the traditional surface EMG signal versus the offline high-density surface electromyography (HDsEMG) signal decomposition. For this study, I used a Graphical User Interface (GUI)which implement Convolutive Kernel Compensation (CKC). This graphical tool allows the operator to decompose the EMG signal and to perform a manual correction of the possible algorithm errors. Thanks to the decomposition approach, the neural activation sent by the spinal cord to the muscles was explored.

The entire analysis is focus on the activity of the tibialis anterior muscle (TA) which was recorded by using a grid of 64 electrodes (HDsEMG). In each experiment, the participants performed 25 isometric ankle dorsiflexion at three different levels of speed (i.e.%MVC/s). In particular, the study consists of two main part:

1. the investigation of the motor units recruitment and the discharge rates modulations to understand how the CNS responds to the different conditions, such as the changing in the contraction speed;

2. the design of two different linear regressor, based on the neural drive and the EMG envelope respectivelly, to estimate the force of the contraction. In particular three single linear regressor (SLR) and the global linear regressor (GLR) were used.

Both the regressions were done considering a time domain feature extracted from the recording force, i.e. the contractile impulse (IC). This was calculated as the integral of the force along time. Thus for both the EMG envelope and the neural drive, the regressions were evaluated with the integral of the signals in each contraction, instead of the signal itself. In order to investigate the performance of the regressors, the R^2 value was evaluated and statistically compared among the different cases.

Even if the results obtained from the two analysis suggest a proportional and linear control via an offline application, a significant statistical difference was found only with the moving window. In particular, a higher R^2 mean values was obtained with the single linear ND model based regressor (${}^{ND_{SLR}}_{mw}R^2_s = 0{,}88$ ${}^{EMG_{SLR}}_{mw}R^2_s = 0{,}80$; ${}^{ND_{SLR}}_{mw}R^2_m = 0{,}87$ ${}^{EMG_{SLR}}_{mw}R^2_m = 0{,}77$; ${}^{ND_{SLR}}_{mw}R^2_f = 0{,}87$ ${}^{EMG_{SLR}}_{mw}R^2_f = 0{,}79$) and the global ND model-based regressor (${}^{ND_{GLR}}_{mw}R^2_g = 0{,}81$ and ${}^{EMG_{GLR}}_{mw}R^2_g = 0{,}69$).

Results suggest that using the HDEMG decomposition similar or even better performance can be achieved for estimating the contractile force of a muscle. Limits of this work, due to time and facilities constraints, are mainly related to the numerosity of subjects involved for the analysis. Future development should also investigate dynamic contractions and different muscles.

Contents

List of Figures v

List of Tables ix

1 Surface electromyogram and recording systems techniques 1

2 Decoding of the motor units activity: perspective for a new neural interface 7

3 Materials and methods 9
3.1 Experimental procedures 9
3.2 Force signal recording 10
3.3 HDsEMG recording 11
3.4 High-density EMG analysis 13

4 Tracking of motor units and analysis of the neural information 15
4.1 Tracking of motor units across different level of force 17
4.2 MUs recruitment order and discharge rate 19

5 Results and discussion of the EMG signal decomposition 23
5.1 Analysis of the CKC inspector results 23
5.2 MU recruitment and firing rate properties 28

6 Contractile impulse estimation 35
6.1 Motor neuron decoding and Neural Drive extraction 36
6.2 Global EMG envelope extraction 40
6.3 Muscular activity onset detection 42
6.4 Linear regressions 42
6.5 Statistical analysis 45

7 Results and discussion 49
7.1 ${}^{ND_{SLR}}_{w}R^2_{s/m/f}$ versus ${}^{EMG_{SLR}}_{w}R^2_{s/m/f}$ 51
7.2 ${}^{ND}_{w}R^2_{g}$ versus ${}^{EMG}_{w}R^2_{g}$ 54

7.3 ${}^{ND_{SLR}}_{mw}R^2_{s/m/f}$ versus ${}^{EMG_{SLR}}_{mw}R^2_{s/m/f}$ 55
7.4 ${}^{ND}_{w}R^2_{g}$ versus ${}^{EMG}_{w}R^2_{g}$ 58
7.5 Statistical analysis: ${}^{ND_{GLR}}_{mw}R^2_{s/m/f}$ versus ${}^{EMG_{GLR}}_{mw}R^2_{s/m/f}$ 59

8 Conclusion and future developments 65

List of Figures

1.1 Representation of three motor neurons and all of their innervated fibers. 1

1.2 In (a) the neural integration of excitatory and inhibitory synapses. In (b) the representation of an AP that travels along the axon to muscle fibers in order to evoke muscle contraction. 2

1.3 In (a) the representation of an individual motor unit with its fibers. Each motor neuron discharge generates an action potential that travels in both muscle fibers directions. In (b) is shown the motor unit action potential (MUAP) that results from the superposition of each muscle fiber action potential (MFAP). 3

1.4 Representation of the neural pulses from the spinal cord to the muscle. Each colored bars represent the motor units discharge timings. The orange arrow is the cumulative spike, that is the combination of all disparages. Adapted from Del Vecchio *et al.* (2019b). 4

1.5 High-density surface electromyography (HDsEMG) signals recorded using a grid of 64 electrodes. The figure shows the evolution over time and space of motor units action potential given by high density systems. Adapted from Merletti *et al.* (2008). 5

3.1 Guided speed protocols. Speed levels: 20%MVC/s ('slow'), 30%MVC/s ('medium'), 60%MVC/s ('fast'). 10

3.2 Adhesive grid of 64-electrodes. 11

3.3 In (a) sEMGs monopolar recordings. Speed level at 20%MVC/s ('slow'). In (b) zooming (dashed rectangle) of one ramp contraction of the entire recording is illustrated. Only one column of the grid of the electrodes is shown. Each row, is one single electrode of the grids. Here, it is shown the sEMGs monopolar recordings for one representative subject. 12

3.4 DEMUSE tool window 13

3.5 The figure shows the CKCreaders structure used in this project. The electrodes grid was reconstructed, sampling frequency of sEMG, montage of electrodes, inter-electrode distance, force signal and the description of the data were defined. 14
3.6 Upper window: motor unit action potential of the selected MU as it is detected by all surface electrodes; central window: instantaneous discharge rate (IDR) including the force as a reference signal (gray line); lower window: train of MU discharge times. A zoom (dashed rectangle) of three ramps contractions including their MU discharge times trains is illustrated. 14

4.1 The surface EMG decomposition provides the number of MUs considering the three levels of speed ramp contraction. In the diagram s, m, f are respectively the number of active motor units found for slow, medium and fast speed of the contraction. Spike triggered averaging (STA) is applied considering all identified MU ($MU_{i:s}$, $MU_{j:m}$, $MU_{k:f}$) and it provides, for each MU its peripheral component (MUAP shepe). To track the same motor unit across different recordings, the MUAP waveforms were cross-correlated across different recordings. In particular, $J*$ and $K*$ contain all the j and k MUs associated with the same i. 16
4.2 An example of the motor unit action potential shape (MUAP) propagation given by the spike triggered averaging technique. 17
4.3 In (a) is shown an example of one resulting tracking and in (b) zooming of four motor unit action potentials inside the dashed box. 19
4.4 Discharge patterns considering three ramp contractions performed at 20%MV/s. Here, 4 MUs are shown (result obtained from the tracking). In (a) MUs are not organized in their recruitment order, while in (b) the same motor units are shown ordered according to their relative recruitment threshold. 22

5.1 Speed of the contraction at 20%MVC/s. 25
5.2 Speed of the contraction at 30%MVC/s. 26
5.3 Speed of the contraction at 60%MVC/s. 27
5.4 20%MVC/s in (a), 30%MVC/s in (b) and 60%MVC/s in (c). Results for one representative subject. 30
5.5 Spread of the recruitment force thresholds for all MUs. Results for one representative subject. 31
5.6 Mean firing rate across the trials considering the three speed of the contraction. In (a) slow speed, in (b) medium speed and in (c) fast speed of the contraction. Results for one representative subject. The MUs are indicated as 1, 2, 3 and 4. 33

6.1 Block diagram of the processing steps for each of the three signal: force, emg envelope and ND. Figure in the left of the block diagram is adapted from (Sartori *et al.*, 2017) 36
6.2 Mask of the low-pass filter. The cut off frequencies is normalized between 0 and 1, where 1 corresponds to the Nyquist rate-half the sample rate. 37
6.3 The process to obtain the cumulative spike train (CST). 38
6.4 The cumulative spike train (CST) in (a) and its continuos-smooted version. Ankle dorsi-flexion performed at 20%MVC/s. 39
6.5 Mask of the band-pass filter. The cut off frequencies is normalized between 0 and 1, where 1 corresponds to the Nyquist rate-half the sample rate. 40
6.6 Trend of raw EMG (orange signal) and its envelope (violet signal) in (a). EMG envelope in (b). Recording performed at 20%MVC/s. . 41
6.7 Results of onset-offset detection using the threshold-based method. Six ramp contractions, normalized to their maximum value, are illustrated: in blue the EMG envelope, in red the neural drive and in orange the recorded ankle dorsiflexion force. In violet the windows of the onset/offset muscular activity. 43
6.8 An example of the regressions designed. The coordinates of each dot on the graph are represented by the time integral calculated under the force curve and the curve of the neural drive (the same description for the EMG envelope). Here, the ramp of 3s (slow speed) is shown. 44
6.9 In (a) the ND model-based estimator, in (b) the EMG envelope model-based estimator. Two examples of the regressions used to estimate the contractile impulse for one representative subject. In (a) and (b) the three single regressions are depicted in different colours: slow speed in yellow, medium speed in red and fast speed in blue. . 44
6.10 Global linear regressor. In (a) ND model-based estimator, in (b) EMG envelope model-based estimator. 45
6.11 In (a) ND model-based estimator, in (b) EMG envelope model-based estimator. Two examples of the regressions used to estimate the contractile impulse for one representative subject considering a moving window of 200ms. In (a) and (b) the three single regressions are depicted in different colours: slow speed in yellow, medium speed in red and fast speed in blue. 45
6.12 Global linear regressor. In (a) ND model-based, in (b)EMG envelope model-based. 46

7.1 The block diagram summarize the R^2 values calculated to asses the performance of the designed regressor. Meaning of pedices and apices are the following: the left subscripts *mw* and *w* indicate respectively *whole* contraction and *moving window*; the right subscripts *s*, *m* and *f* indicate respectively *slow*, *medium* and *fast* speed of the contraction, The subscript on the left *GLR* and *SRL* indicate respectively the global and single linear regressor; finally the superscripts *ND* and *EMG* indicate respectively the neural drive and the EMG envelope to underlay the model used. 50
7.2 Two examples of the regressions for the ND model-based. The regressions for the three speed of the contraction are depicted in different colours: slow speed in yellow, medium speed in red and fast speed in blue. The results shown are for two representative subjects. . . . 51
7.3 Two examples of the regressions for the EMGe envelope model-based The regressions for the three speed of the contraction are depicted in different colours: slow speed in yellow, medium speed in red and fast speed in blue. The results shown are for two representative subjects. 52
7.4 Boxplots showing the ranges of R^2 obtained with the linear regressors. 53
7.5 In (a) total regressor based on 7.2 (a). In (b) total regressor based on 7.3 (a). 54
7.6 Boxplots showing the ranges of R^2 obtained with the global regressor 54
7.7 Four examples of the regressions used to estimate the contractile impulse. In (a) and (b) the ND model-based; in (c) and (d) the EMG envelope model-based. The regressions for the three speed of the contraction are depicted in different colours: slow speed in yellow, medium speed in red and fast speed in blue. The results shown are for two representative subjects. 55
7.8 Boxplots showing the ranges of R^2 obtained with the single linear regressors. According to the convention symbol used in statistic, * indicates a p value < 0.05 while ** indicates a p value < 0.01. . . . 57
7.9 In (a) the global regressor obtained with the ND model-based; in (b) the global regressor obtained with the EMG envelope model-based. 58
7.10 Boxplot shows the ranges of R^2 obtained with the global regressor. According to the convention symbol used in statistic, ** indicates a p value < 0.01. 58
7.11 Boxplots showing the ranges of R^2 obtained with the global regressor In (c) there is no significance statistical difference. 60
7.12 Boxplots showing the ranges of R^2 obtained with the global regressor and the single linear regressions using the EMG model-based. . . . 62
7.13 Boxplots showing the ranges of R^2 obtained with the global regressor and the single linear regressions using the ND model-based. 63

List of Tables

4.1 Final number of the tracked MUs across contractions spanning at different %MVC range (20 %MVC/s, 30 %MVC/s, 60 %MVC/s). Mean and standard deviation for the finding cross-correlation values. 18
4.2 Recruitment order/sequence for subject 1 during medium contractions (30%MVC/s). 20

5.1 Number of decomposed motor units per subject. 24
5.2 Recruitment order for subject 1 during slow contractions (20%MVC/s). 29
5.3 Recruitment order for subject 1 during fast contractions (60%MVC/s). 29
5.4 Recruitment order for subject 1 during medium contractions (30%MVC/s). 29
5.5 Average motor unit recruitment threshold (%MVC) per subject. Only 2 participants out of 7 showed an higher recruitment threshold in fast compared to slow contractions (highlighted). 32

7.1 R^2 considering the entire ramp contraction for each single linear regression. Values per subject. 52
7.2 R^2 considering 200ms window. Values per subject. 56
7.3 R^2 considering the estimation of the global model for each different speed. Values per subject. 59
7.4 R^2 considering 200ms window. Values per subject. Table on the left indicates the R^2 for the each SLRs, while the table on the right indicates the R^2 obtained estimating each single force by the GLR. 61
7.5 R^2 considering 200ms window. Values per subject. Table on the left indicates the R^2 for the each SLRs, while the table on the right indicates the R^2 obtained estimating each single force by the GLR. 61

Chapter 1

Surface electromyogram and recording systems techniques

The main effector of the human musculoskeletal system is the muscle, which enables all voluntary (e.g. walking, grasping, ...) and involuntary (e.g. hear beating, ...) movement. These movements are in turn promoted and consequently tuned by the central and peripheral nervous system through different complex mechanisms. In this complex scenario, the motor unit (MU) is presented. The motor unit is considered the smallest functional unit of the neuromuscular system and it is made up of a α motor neuron and the skeletal muscle fibres innervated by the motor neuron. The motor neurons are situated in the ventral horn of the spinal cord, with its cell body and its dendrites, while its axon projects outside of the spinal cord towards the targeted muscle (Heckman & Enoka, 2012). Motor neuron could projects its axon on several fibres of a muscle, while a single muscle fibre can be innervated only by a single motor neuron (see Fig. 1.1).

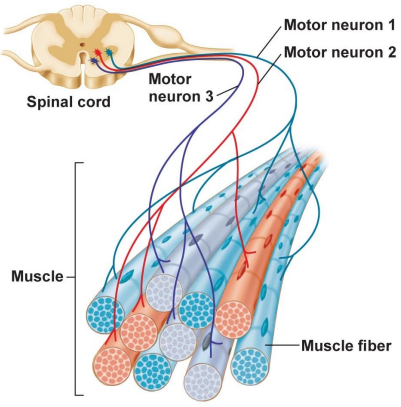

Figure 1.1. Representation of three motor neurons and all of their innervated fibers.

These anatomical characteristics are extremely important to control and coordinate the muscle contraction, e.g. in terms of force, stiffness and velocity of movements. The activation of the motor neuron mainly depends on the input received. In fact, it is composed by multiple processes, called dendrites, that are located inside the spinal cord and extend for up to 2 mm from the cell body (Heckman & Enoka, 2012). These processes receive several excitatory and inhibitory synaptic input (see Fig. 1.2) from the cortex, the brainstem and the peripheral sensory receptors (Binder *et al.*, 1996; Fyffe, 2001). These descending and reflex inputs determine whether or not a neuron should be active.

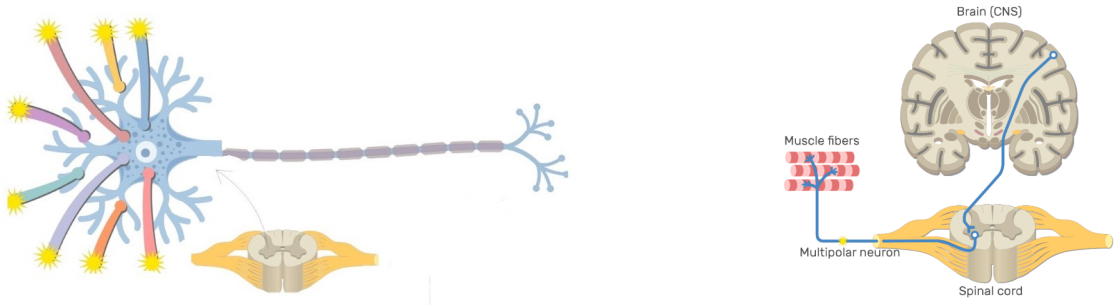

(a) (b)

Figure 1.2. In (a) the neural integration of excitatory and inhibitory synapses. In (b) the representation of an AP that travels along the axon to muscle fibers in order to evoke muscle contraction.

The motor neuron activation is determined by the sum of the depolarizing and hyperpolarizing inputs. When this sum exceeds the motor neuron specific threshold, an action potential is generated (AP).

The action potential is generated at the spinal level and it is transmitted through the axon to the neuromuscular junction where it is transmitted to all of the innervated fibres (Heckman & Enoka, 2004). Each discharge can generate a fiber action potential, defined as Muscle Fiber Action Potential (MFAP) that propagates in both fibers directions (see Fig. 1.3(a)). The generation of different AP from all muscle fibers innervated by the same motor neuron, overlap in time and generate the motor unit action potential (MUAP) (see Fig. 1.3(a)). Because the motor neuron fires repetitively to obtain a certain contraction, the ensemble of several firings generates the motor unit action potential trains (MUAPTs). The interference signal recorded with two or more surface electrodes consists of a superposition of the MUAPTs from all of the MU's activate and detected by the acquisition systems (see Fig. 1.3(b)). Thus, the spatial and temporal summation of several MUAPTs from the recruited MUs represents the electromyogram (EMG) or myoelectric (ME) signal (Lefever & De Luca, 1982).

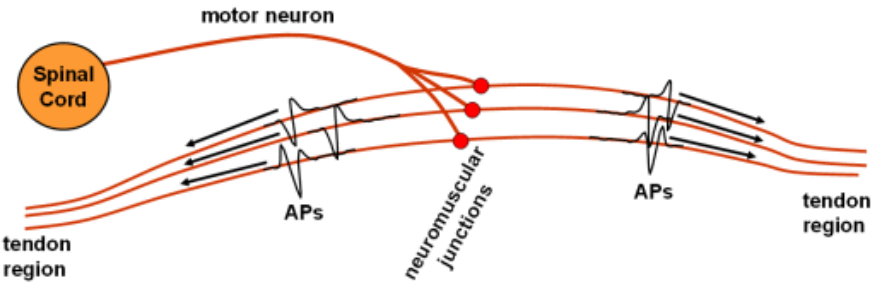

(a)

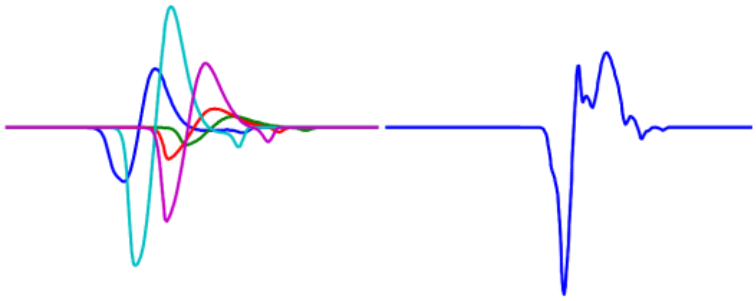

(b)

Figure 1.3. In (a) the representation of an individual motor unit with its fibers. Each motor neuron discharge generates an action potential that travels in both muscle fibers directions. In (b) is shown the motor unit action potential (MUAP) that results from the superposition of each muscle fiber action potential (MFAP).

The motor neuron discharges are assimilated to a sequence of electrical pulses (IPTs) (see Fig. 1.4) directly proportional to the amount of the synaptic inputs sent to the motor neuron pool (Kernell, 1992). The combination of these IPTs, from different MUs, is defined as the cumulative spike train (CST) and it is considered a reliable estimate of the neural drive sent by the spinal cord to all motor units within the same muscle.

The motor neurons that innervate the same muscle constitute the motor pools (Burke *et al.*, 1977), but each motor neuron is different from the others in terms of electrical properties and of the relative amplitudes of the inputs that it receives. A pool of motor neurons usually comprise about 100 motor neurons for small muscles, to approximately 1000 motor neurons for large muscles (Heckman & Enoka, 2012).

The muscle fibres are classified in three distinct types. This distinction depends on their contractile and energetic properties. In particular, it is possible to discriminate between type I, type IIa, type IIx fibers (Heckman & Enoka, 2012). This discrimination is based on myosin ATPase activity. A second classification is based on the velocity of the contraction. There are three different type of fibers: type S, type FR, type FF.

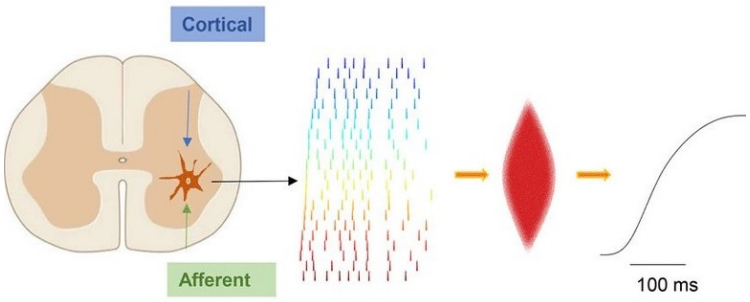

Figure 1.4. Representation of the neural pulses from the spinal cord to the muscle. Each colored bars represent the motor units discharge timings. The orange arrow is the cumulative spike, that is the combination of all disparages. Adapted from Del Vecchio *et al.* (2019b).

The first type of muscle fibres is defined as slow-twitch because of their reduced contraction speed compared to the fast-twitch fibres (FR and FF) (Heckman & Enoka, 2012). In addition, it is possible a discrimination according to the fatigability, that is the capacity to produce force as a response to a continuous excitation. According to this, the type S fibers are fatigue resistance thus the MUs characterised by these fibers are recruited for slow contraction, while the MUs characterised by FR and FF fibers are recruited for fast contraction because these fibers are fatigue resistant. Thanks to this differentiation, the CNS can control and modulate the force that a specific muscle can exert, by recruiting different kind of MUs. The MUs are recruited orderly according to Henneman's size principle (Heckman & Enoka, 2004), that is from the smaller to the larger diameter motor units. In particular, the CNS regulates the force in two different ways: temporal and spatial recruitment. The temporal recruitment is based on the discharge rate of the motor unit: the more force is required the higher is the firing rate. Indeed, the MUs discharge rate varies from 8 to 5 pulse/s (pps) but it can achieve values up to 100-200 pps during brief rapid contractions (Heckman & Enoka, 2012; Van Cutsem *et al.*, 1998). The spatial recruitment regards the recruitment of additional motor units to generate more force. It is clear now, how the neural command from the CNS tunes the muscle activity through the motor units. This means that the central information can be investigated measuring directly the EMG signal. To do this, different technologies have been developed. One of the most used classification for these systems divides them in two category: intramuscular electrodes and surface electrodes.

The intramuscular electrodes detect the EMG activity using needles or wires inserted in the muscles (Duchateau & Enoka, 2011). In this way, the intramuscular recording is able to follow the electrical potential at the muscle fibres source (Stoykov *et al.*, 2005). This is quite important since it provides to obtain information regarding the physiological properties of MUs and it permits clinical investigations (Merletti & Farina, 2009) such as the diagnosis of myopathies or diseases of the α motor neurons. This method of recording is characterized by a high selectivity since it gives the possibility to directly measure the single motor unit action potentials. On the contrary, the main drawback is represented by its invasiveness. In addition, with this technology we can monitor only few MUs concurrently (Muceli *et al.*, 2015). Advances in fabrication allowed to expand the number of concurrently motor units using non-invasive techniques.

Surface electrodes are the recording systems that allow to acquire the EMG signals placing the electrodes over the skin. Surface electrodes are distinguished into single-channel bipolar recording and high-density systems of closely spaced electrodes (HDsEMG) (H. Blok *et al.*, 2002). The main difference between the standard single-channel bipolar recording and HDsEMG is in the information that they provide. A grid of electrodes provides a signal that has two spatial and one temporal dimension (see Fig. 1.5) with respect to one-dimensional signal given by the single-channel (Merletti *et al.*, 2008).

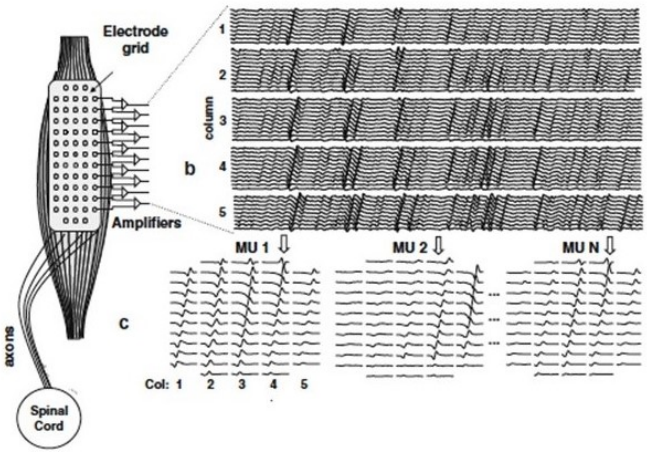

Figure 1.5. High-density surface electromyography (HDsEMG) signals recorded using a grid of 64 electrodes. The figure shows the evolution over time and space of motor units action potential given by high density systems. Adapted from Merletti *et al.* (2008).

Despite the HDsEMG provides a spatial sampling because it detects signals in multiple locations, using the amplitude of the EMG to estimate the neural information sent to the muscle may result in a wrong estimation. This is due to the fact that the EMG amplitude is influenced by several factors as the amplitude cancellation (Keenan *et al.*, 2006), that is the result of the algebric summation of positive and negative phases of action potentials (Day & Hulliger, 2001). This phenomenon, underestimates the amplitude of the EMG signal and makes it a poor indicator of the neural activation (Farina *et al.*, 2010). In addition, the amplitude cancellation may influence low threshold MUs action potential because they produce smaller APs (Kallenberg & Hermens, 2006). In this case, the surface EMG signal results less sensitive to the changes in the activity of low-threshold motor units. Finally the amplitude cancellation may mask the action potentials waveforms that may change across conditions, such as during fatiguing contractions. Indeed, in these conditions, different adjustments may be actuated by the central nervous system that are reflected and thus detectable in AP waveforms (Dimitrova & Dimitrov, 2002). All of these issues imply that the action potential shape have a significant influence on the results (Farina *et al.*, 2010). In order to estimate the neural drive sent by the spinal cord to muscle, the identification of the discharge times is explored.

Chapter 2

Decoding of the motor units activity: perspective for a new neural interface

The surface electromyogram (EMG) is used in several studies related to clinical neurophysiology, rehabilitation research, sport sciences, kinesiology and ergonomics (Hogrel, 2005). In clinical applications it is the standard method to evaluate neurophysiological characteristics of neuromuscular diseases (Drost *et al.*, 2006). For instance, by using the HDsEMG, it is possible to conduct fatigue studies in neuromuscular disorders, motor neuron diseases (MND) and neuropathies. However, the use of HDsEMG is also a useful instrument to investigate the interaction between the neuromuscular and the musculoskeletal systems.

With the aim to understand the human movement, a knowledge of the mechanisms underlying the neural functions is needed. In this perspective the purposes of this thesis are placed. In particular, the relationship between the spinal motor neurons activity and the muscle force produced is explored. This study has been focused on isometric ankle dorsi-flexion contractions performed at different speed of the contraction, considering one single joint angular position. The decoding of the α- motor neuron discharges allows an estimation of the contractile impulse to the muscle. In particular, a simple linear regression is applied both to the motor unit model-based and EMG model-based. The regressions point out and explore the difference between the current myoelectric control methods, based on the EMG amplitude and the perspective for a new human-machine interfacing. The new human-machine interfacing has the aim to decode the neural signals, to process them and to extract the the user's intent (Farina *et al.*, 2017). Nowadays, the human/machine interface indirectly detects the efferent activity by electrodes placed on the muscle structures above the amputation; in this way from the surface EMG signals time-and frequency-domain features are extracted (Kapelner *et al.*, 2018) for either control or identify sets of predefined movements (Farina *et al.*, 2017).

Because the global EMG is a spatial temporal summation of action potentials, its amplitude is an approximation of the neural impulse to the effective force muscle production (Twardowski *et al.*, 2019). Using the neural signal, which means to identify the occurrences of motor unit action potentials (MUAPs), it would allow to separate the neural information from the peripheral information (Twardowski *et al.*, 2019). These, together with the crosstalk and the amplitude cancellation (De Luca & Merletti, 1988), represent the peripheral contribution that mask the neural drive. In this way, by decoding the output spike trains of the spinal motor neurons, it is possible to map the activity of a large number of motor neurons into a command needed for myocontrol. In addition, the idea to decompose the EMG signal, allows to investigate the underlying processes of its generation (Kapelner *et al.*, 2019). Decoding the motor neuron behaviour provides to explore both the motor unit firing rates and their recruitment which are the natural physiological mechanisms for controlling force and movement of the limbs (De Luca & Erim, 1994). This new scenario is made possible by the decomposition systems that, from the interference EMG, recuperate the motor neuron activity and thus the neural drive to the muscle. The neural drive is a direct estimation of the total spinal cord activity, which is possible to estimate by the total number of the discharges given by the identified motor neurons.

In this thesis, the approach used to obtain motor units and their discharges, is the convolutive blind source separation method (Holobar & Zazula, 2007). This method considers the multi-channel EMG signals as a convolutive mixture of sources (Kapelner *et al.*, 2019) (partly correlated) where the mixing process is unknown. Therefore, it is needed to decompose the EMGs signal blindly (Holobar & Zazula, 2007) in their series of motor unit discharge timings (sources).

In particular, the motor unit discharge timings can be described as a set of delta functions where the impulse responses of the filters is represented by the MUAPs (Negro *et al.*, 2016). In this way, each EMG channel sees the series of motor-neuron discharge timings as a filter version resulting from the motor unit action potentials (Farina *et al.*, 2017). Each MUAP is a different filter where the shape is unknown because it is function of space, muscle properties, volume conductor characteristics and the acquisition system properties (Holobar & Farina, 2014). The aim is to extract the motor unit discharge timings in order to associate them to each individual motor neurons. What makes the use of the discharge timings fascinating and new, compared to the extracted time-frequency domain EMG features, it is the fact that the occurrences are the natural neural code sent from the spinal cord to the muscle while the neural drive is the result of their combination. In conclusion, the possibility to study the contribution of the motor neuron activity opens new avenues both to improve neuro-prosthetic interfaces by developing a bio-inspired and more flexible control, but also in the understanding of neuro-mechanical causalities in human movement or in the alterations caused by impairment (Sartori *et al.*, 2017).

Chapter 3

Materials and methods

Seven healthy volunteers, five males and two females, (men and females aged 20-28) with no previous history of neuromuscular disorders or lower limb pathology took part in the study. An informed consent outlining experimental procedures was signed by all the volunteers before their involvement. sEMG signals were recorded in the laboratory of University College London (UCL) in June 2018. The study was approved by the ethical committee of the Bioengineering Department, University College London (UCL). The experimental investigation was held at Prof. J. Rothwell's Physiology and Pathophysiology of Human Motor Control Laboratory. The data were acquired for a previous master thesis work, with aim to investigate MRCPs associated with up to three levels of rate of force development (RFD). Before the experiment, testing procedures and protocols have been explained to volunteers. Then, baseline measurements were obtained. These have included the recordings of ankle dorsiflexion forces during maximal and submaximal voluntary contractions and high-density surface EMG (HDsEMG) recordings from the tibialis anterior (TA) muscle.

3.1 Experimental procedures

The main task involved the recordings of muscle force and surface HDsEMG signals from the TA muscle of the dominant leg during isometric contraction performed at three different levels of speed or rate of force development (RFD). In this study, the RFD was calculated as the slope of the force time curve (N/s). Then it was normalized for the maximum voluntary contraction (MVC) (%MVC/s). After the familiarization session, approximately 5 min, each participant was asked to focus on the movement of the ankle dorsi-flexion in order to isolate TA activa- tion as much as possible. Each experimental session started with the collection of three maximum voluntary contractions (MVC). The peak force achieved were displayed on a monitor; then the maximal voluntary force (MVF) was defined as the highest

force recorded during the MVCs measurements. This value was used as a reference. Each participant performed approximately 25 isometric ankle dorsi- flexions, interspersed with 5s of resting periods. Each trial lasted 15s, overall. In between different tasks, resting intervals of 5 min were given. The experiments lasted approximately 40 min. During the submaximal contractions, the volunteers performed three types of visually assisted dorsi-flexions per protocol reaching a predefined target value equal to 60% ±5% of their MVF and a then back to the resting value. In each trail, the duration of each phase was varied proportionally (1s, 2s, 3s), thus the speed to perform the ramp contraction increased (see Fig. 3.1): 20%MVC/s ('slow'), 30%MVC/s ('medium'), 60%MVC/s ('fast'). Each ramp contraction was performed at the same ankle joint (one degree of fredoom (DoF)). Visual feedback guided the participants throughout the experiment (custom-made graphical user interface (Knud Larsen, SMI, Alborg University)).

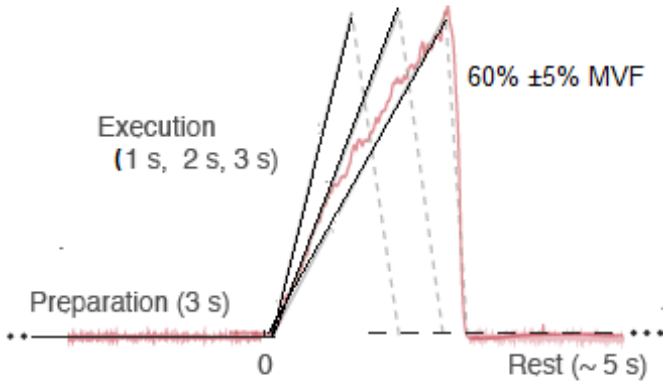

Figure 3.1. Guided speed protocols. Speed levels: 20%MVC/s ('slow'), 30%MVC/s ('medium'), 60%MVC/s ('fast').

3.2 Force signal recording

The experimental set-up comprised a custom-made ankle ergometer (OT Bioelettronica, Turin, Italy) that was fixed to an examination table with two adjustable straps. Each volunteers was seated comfortably on a seat, with the dominant leg secured with straps at the foot, ankle and knee (Del Vecchio *et al.*, 2019a). To record the force, the hip was flexed at 120° (180° = supine position), the knee extended to 180° (supine position) and the ankle was placed at 100° (90° = perpendicular to the tibia) of plantar flexion (Del Vecchio *et al.*, 2019a). The foot was positioned under

a custom-made pedal, calibrated load cell (CCT Transducer s.a.s, Turin Italy). The analogue force signal, recorded from the load cell was amplified (200×) and sampled at 2048 Hz via an external analogue-to-digital converter (EMG-Quattrocento; OTBioelettronica, Turin, Italy). The force signal was recorded with the software OTbiolab (OT Bioelettronica) and visual feedback was provided with Labview, version 8.0 (National Instruments, Austin, TX, USA). During offline analysis, the force signal was converted to newtons (N), the offset was gravity corrected and it was low pass filtered (Butterworth, third order, cut-off frequency 20Hz).

3.3 HDsEMG recording

HDsEMG signals were recorded from the TA with one adhesive grid of 64-electrodes (see Fig. 3.2) (gold-coated; diameter 1 mm; inter electrode distance 8 mm; OT Bioelettronica) located at the distal portion of the muscle. The skin in the proximity of the TA muscle was shaved, lightly abraded and cleansed with 70% ethanol, prior to placing the grid with conductive paste. Then, the perimeter of the muscle was identified in order to placed the electrodes grid. The adhesive grids was placed over the muscle using bi-adhesive perforated foam layers (SpesMedica, Battipaglia, Italy). To optimize the skin-electrode contact the cavities of the adhesive layers was filled with conductive gel (SpesMedica) (Del Vecchio *et al.*, 2019a). The ground electrode was dampened with water and it was placed on the styloid process of the ulna of the arm. Two reference electrodes were positioned on the tuberositas tibialis and on the medial malleolus of the dominant leg (Del Vecchio *et al.*, 2019a). The HDsEMG signals were recorded in monopolar derivation (see Fig. 3.3) with a sampling frequency of 2048 Hz, amplified (150×) and band-pass filtered (10–500 Hz). The analog signals were converted to digital data using a multichannel amplifier with 16-bit resolution (3 dB bandwidth, 10–500 Hz; EMG-Quattrocento; OT Bioelettronica).

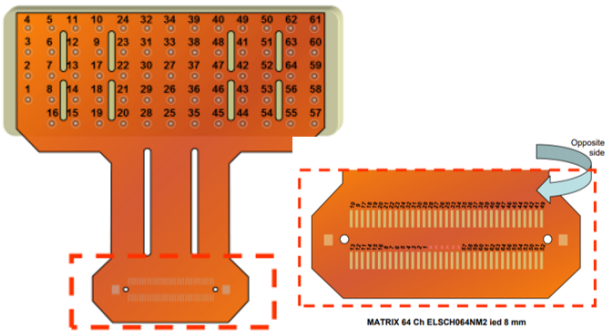

Figure 3.2. Adhesive grid of 64-electrodes.

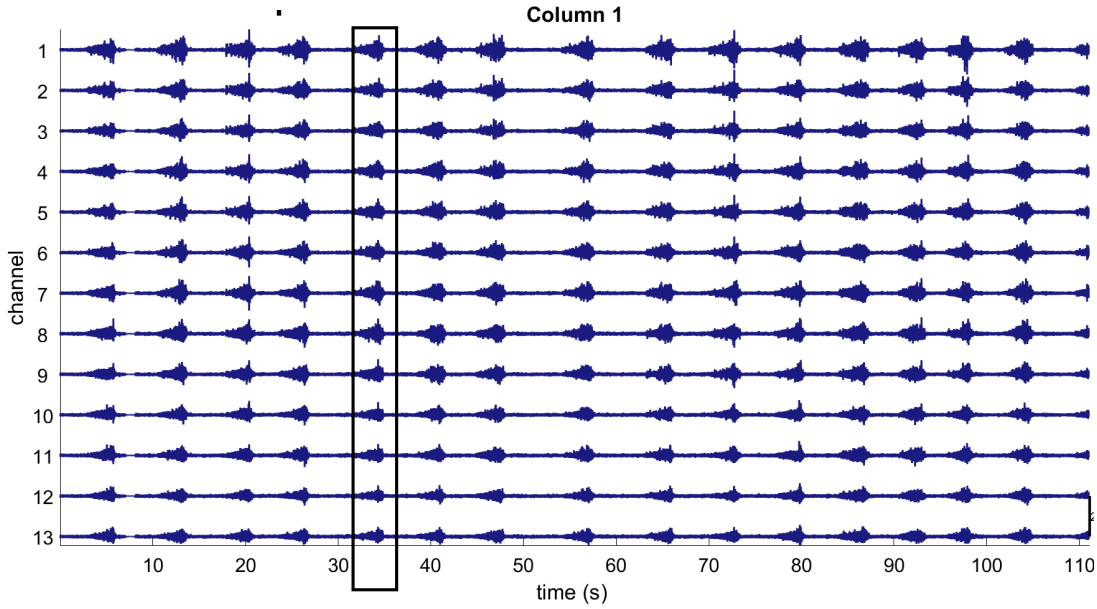

(a)

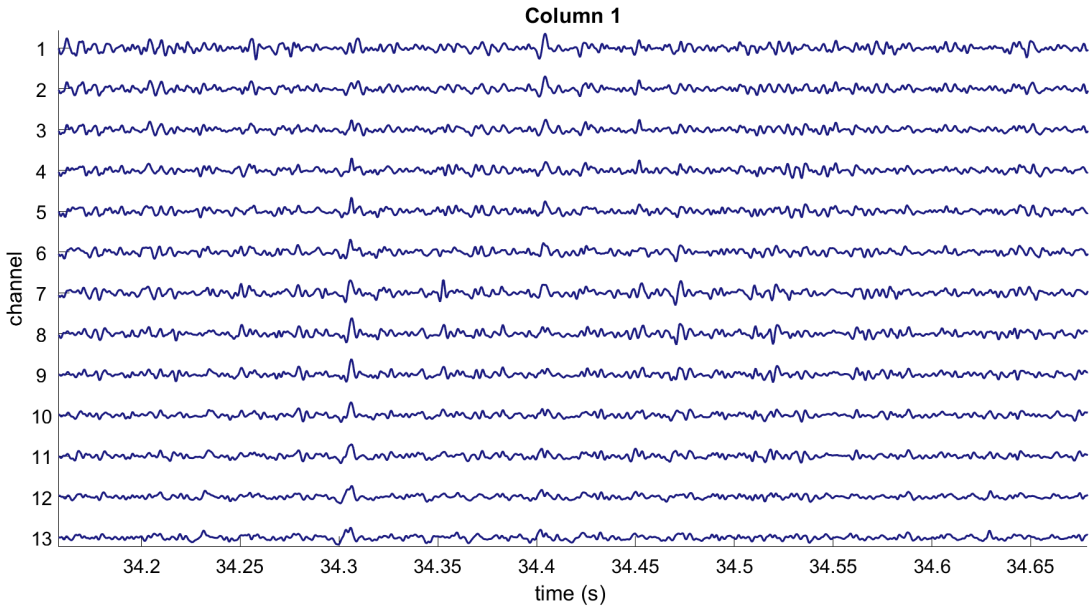

(b)

Figure 3.3. In (a) sEMGs monopolar recordings. Speed level at 20%MVC/s ('slow'). In (b) zooming (dashed rectangle) of one ramp contraction of the entire recording is illustrated. Only one column of the grid of the electrodes is shown. Each row, is one single electrode of the grids. Here, it is shown the sEMGs monopolar recordings for one representative subject.

3.4 High-density EMG analysis

DEMUSE is the graphical user interface (GUI) (see Fig. 3.4), based on the Convolutive Kernel Compensation (CKC) (Holobar & Zazula, 2007) used in the present work to obtain the offline HDsEMG signals decomposition. This tool runs in MATLAB environment and it is an automatic signal decomposition algorithm.

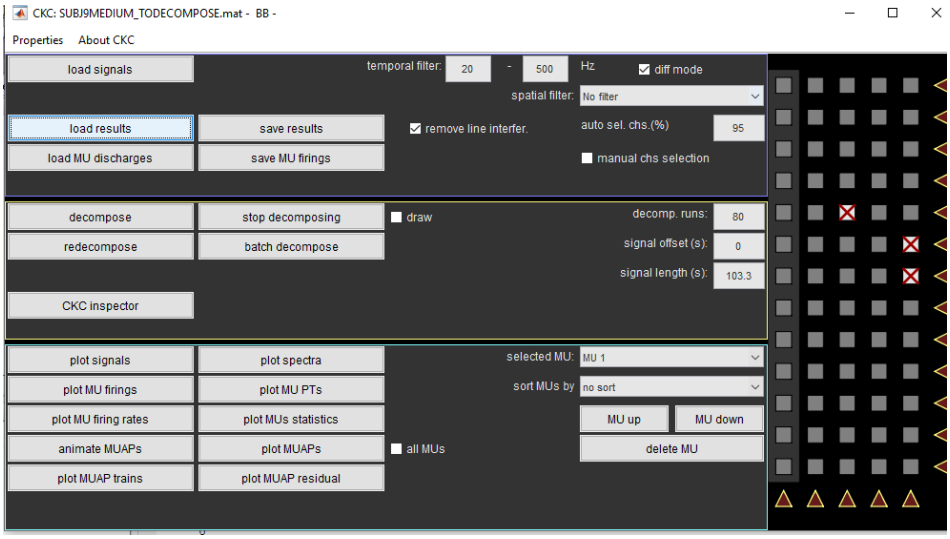

Figure 3.4. DEMUSE tool window

Before to load the EMGs data, a proper reader defined as *CKCreader* in form of MATLAB (*.mat*) structure was created (see Fig. 3.4). All of the *CKCreader* specify the same inputs and output. Then, the sEMGs were loaded and the automatic algorithm provided to their automatic decomposition; only the number of decomposition runs (this value was set to 80), the initial offset (this value was set to 0) and the length of EMG time interval to be decomposed (this value was set to 111) are specified by the user. In this work the percentage of the EMG channels to be included into the decomposition was left to the default value (95 %). *DEMUSE* uses a band-pass filter (Butterworth, 2nd order) to filter the raw EMG signals with a default cut-off frequencies set to 20 Hz and 500 Hz. In addition this automatic decomposition tool removes the line interference and it tests the acquired EMG channels both for the presence of movement artefacts and for the bad skin-electrode contacts. Thus the button (*decompose*) provides the EMG signal decomposition. When the decomposition ends, it is possible to visualize the results.

Despite *DEMUSE* is an automatic tool, it allows the manual inspection of the decomposition results thanks to the button *CKC inspector*. The manual user inspection consists in the addition or in the deleting of MU discharges but it is also

possible to check and to delete MUs which are repeated. Since*DEMUSE* calculates the Pulse-to-Noise Ratio (PNR) metric for each identified motor unit, the accuracy in motor unit identification was set to 30 dB. Thus, MUs that shown a PNR > 30 dB (Holobar *et al.*, 2014) were stored for further analysis.

The results of the decomposition were plot in MATLAB and they are discussed in terms of instantaneous discharge patterns, smoothed MU discharge rates and multichannel MUAPs in Chapter 5.

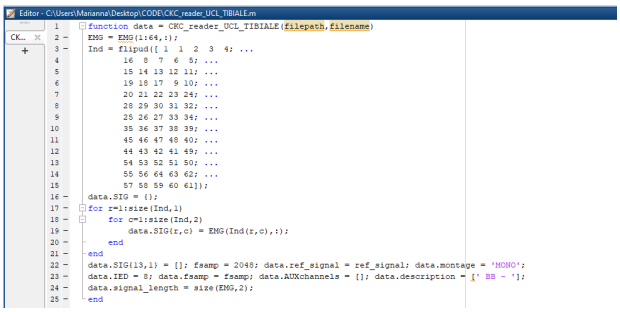

Figure 3.5. The figure shows the CKCreaders structure used in this project. The electrodes grid was reconstructed, sampling frequency of sEMG, montage of electrodes, inter-electrode distance, force signal and the description of the data were defined.

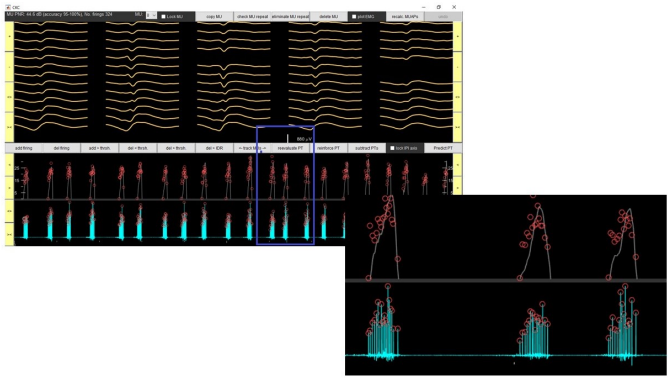

Figure 3.6. Upper window: motor unit action potential of the selected MU as it is detected by all surface electrodes; central window: instantaneous discharge rate (IDR) including the force as a reference signal (gray line); lower window: train of MU discharge times. A zoom (dashed rectangle) of three ramps contractions including their MU discharge times trains is illustrated.

Chapter 4

Tracking of motor units and analysis of the neural information

In order to investigate the interaction between the neuromuscular and the musculoskeletal systems, an algorithm to track the same motor units (MUs) across different %MVCs/s was implemented. The idea to follow the same MU allows to understand whether the CNS has any preferential motor unit recruitment sequence to perform the same task across different conditions, i.e. different contraction speed. In addition, the possibility of identifying the same motor units over different experimental sessions provides new perspectives for studies in neuromuscular adaptations (Martinez-Valdes *et al.*, 2017) and in the understanding of differences between high and low threshold MUs in the force control. In this way, the relationship between force and spinal motor neurons activity is exhaustively explored, taking into account at the same time how the firing rate of each single motor unit is modulated (mean discharge rates) and how motor units are recruited by the CNS to achieve precise and complex movements.

The block diagram in Fig. 4.1 summarizes the processing steps on which the implemented algorithm is based.

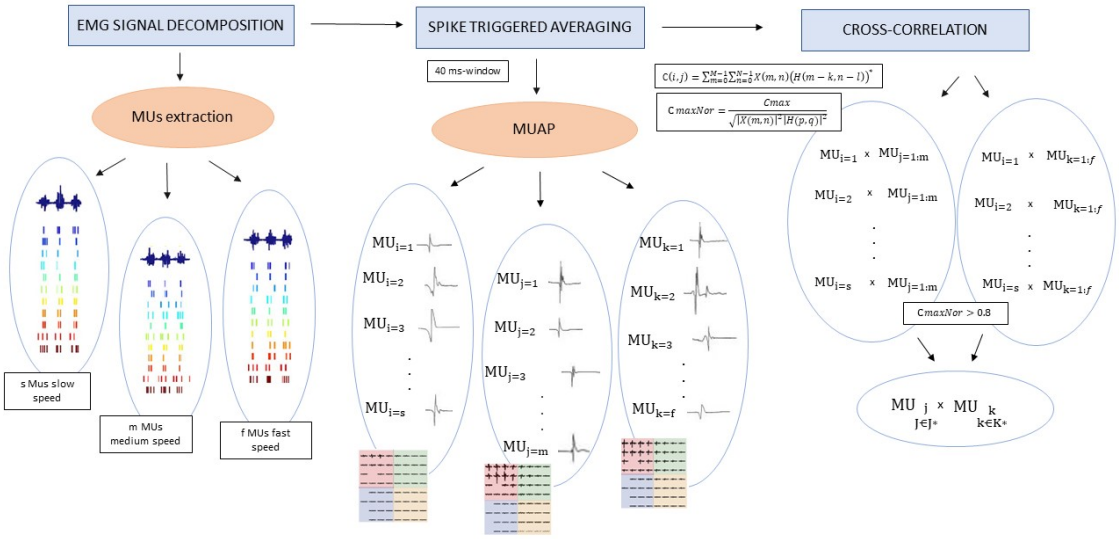

Figure 4.1. The surface EMG decomposition provides the number of MUs considering the three levels of speed ramp contraction. In the diagram s, m, f are respectively the number of active motor units found for slow, medium and fast speed of the contraction. Spike triggered averaging (STA) is applied considering all identified MU ($MU_{i:s}$, $MU_{j:m}$, $MU_{k:f}$) and it provides, for each MU its peripheral component (MUAP shepe). To track the same motor unit across different recordings, the MUAP waveforms were cross-correlated across different recordings. In particular, $J*$ and $K*$ contain all the j and k MUs associated with the same i.

4.1 Tracking of motor units across different level of force

With the aim to track the same MU at the three different speeds of contraction(20 -30 -60 %MVC/s), we calculated the single differentials subtracting adjacent monopolar signals. The resulting signals were band-pass filtered at 20–500 Hz (Butterworth, order 3). HDsEMG signals decomposition provide access to the discharge times for all MUs identified by blind source separation algorithm based on deconvolution (CKC). To obtain the motor unit action potentials waveforms, spike triggered averaging (STA) technique was used. This technique consists in averaging the segments (40 ms-windows) of each EMG channel around the time occurrences of the constituent motor unit firings to obtain an averaged MUAP for each EMG channel of the recording matrix (see Fig. 4.2). MUAP waveforms are used to track

Figure 4.2. An example of the motor unit action potential shape (MUAP) propagation given by the spike triggered averaging technique.

the same motor unit across different recordings by similarity matching. The similarity across the recordings was computed through cross-correlation analysis. The cross correlation was calculated using the MATLAB function *xcorr2*. This function returs a 2-D cross-correlation matrix. In signal processing, the cross-correlation is a measure of the similarity between two waveforms as a function of a time-lag applied to one of them. In Eq. 4.1 is reported the mathematical expression to calculate

the cross-correlation between to matrix:

$$C(k,l) = \sum_{m=0}^{M-1} \sum_{n=0}^{N-1} X(m,n)(H(m-k,n-l))^* \tag{4.1}$$

where X (MxN) and H (PxQ) are the two input signal matrices, while C is the output matrix. Since the cross-correlation has its maximum value, C_{max}, when the two input matrices are aligned, this value is taken as the result of their similarity. Then the maximum value of the coefficient was normalized to limit its value in the range between -1 and 1.

$$MaxNorm = \frac{C_{max}}{\sqrt{\mid X(m,n) \mid^2 \mid H(p,q) \mid^2}} \tag{4.2}$$

Similar MUs were coupled across pairs of recordings to create a chain of similar MUs, aiming to concatenate the activity of the same MU across the three different contractions. To assess a sufficient similarity and guarantee a certain accuracy of the tracking procedure, a cross-correlation threshold was set (CC $>$ 0.8) (Martinez-Valdes *et al.*, 2017). MUs were matched considering two recordings at the same time, e.g. 'Fast'-'Slow' and 'Fast'-'Medium'.

To track the same motor units across contractions with different speeds, the common speed with respect to previous matching was considered (in the example shown, 'Fast') (see Fig. 4.1). Thus, the resulting final chain is composed only by motor units that are present simultaneously in the matching that includes the common speed. The resulting matching is shown in Table 4.1.

Subject	**MUs**	**Cross value**
1	4	0.84 ±0.03
2	4	0.88 ±0.04
3	10	0.96 ±0.03
4	5	0.93 ±0.01
5	12	0.94 ±0.03
6	4	0.93 ±0.01
7	3	0.93 ±0.04

Table 4.1. Final number of the tracked MUs across contractions spanning at different %MVC range (20 %MVC/s, 30 %MVC/s, 60 %MVC/s). Mean and standard deviation for the finding cross-correlation values.

The results show how a high threshold motor unit may be recruited both during slow and rapid movements. This means that in all contraction speeds investigated in the present study (20 %MVC/s, 30 %MVC/s, 60 %MVC/s), MUs recruitment may act with the same mechanism.

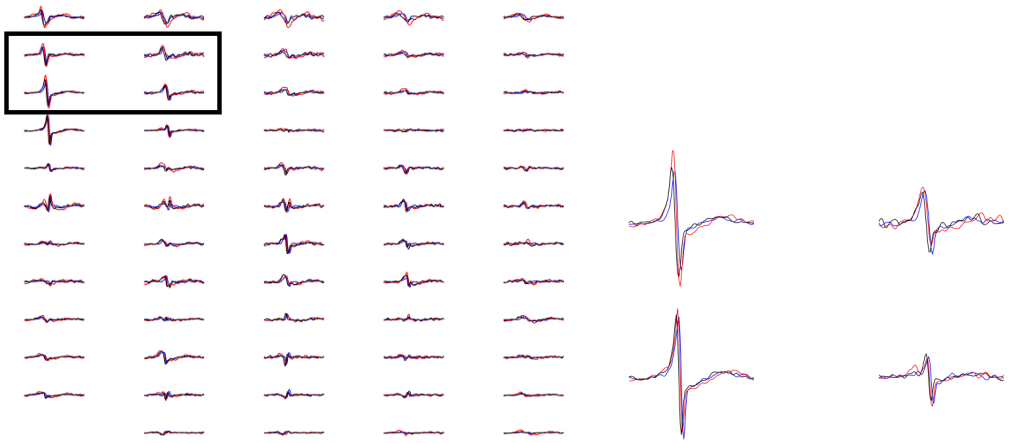

(a) (b)

Figure 4.3. In (a) is shown an example of one resulting tracking and in (b) zooming of four motor unit action potentials inside the dashed box.

The reliability of the current outcome (see Fig. 4.3) is given by the EMG recording system itself (i.e. HDsEMG) used in the present study. Indeed, Farina *et al.* (2008) demonstrated that by using a large number of channels, it is possible to identify the single MU activity and thus to exclude the possibility that, different motor units, show identical waveform shapes. Further analysis regarding the neural information are conducted considering only the tracked MUs.

4.2 MUs recruitment order and discharge rate

The neural information extracted by the decomposition procedure allows to investigate the neural strategies of control of muscle contractions. The output of the HDsEMG decomposition procedure is a file containing the number of motor units identified and the relative discharge timings. The individual discharge timings were converted to binary spike trains: 0 or 1 were assigned to each sample depending on the presence/absence of a discharge timing. Since the *CKC inspector* output does not give the MUs in their order of recruitment, but the output is organized based on the first MU identified, it was necessary to determine the recruitment order. Motor unit recruitment threshold represents the force (N) at which the motor neuron began to discharge action potentials. Therefore the first discharge timing and the correspondent level of force were stored for each motor unit within each contraction and for each participant. Thus, the MUs were ordered from the first recruited to the last (see Fig. 4.4). MU recruitment was investigated in the same recording (single trial) and across the trials performed to understand if any change

in recruitment threshold occurred across contractions at the same speed, and at the three different velocities, e.g. MU_1 is always the first recruited. Thus, the number of all possible recruitment permutations was explored. Permutation defines all possible ways of arranging members that compose a set considering the specific order in which the objects will be organized. To find all possible permutation the MATLAB function *perms* was used.

The mathematical model that explains the above definition is:

$$P_r^n = \frac{n!}{(n-r)!} \tag{4.3}$$

Because in this case $n = r$, the equation 4.3 became:

$$P_r^n = n! \tag{4.4}$$

where n represents the MUs and r is the position on the recruitment order.

Because the function *perms* returns a matrix containing all permutations of the elements of the input, in P_r^n there are also groupings that were not present across the trails performed at the same %MVCs. For this reason, in the output matrix, only the real recurring groups were found. In this way, it was taken into account how many times, a certain recruitment order, was presented during the recording (see Table 5.4: each column is a possible recruitment order. The last row reports how many times that order characterized the entire recording). Considering the medium speed of the contraction (see Table 5.4), we observed six recurrent recruitment sequences and the entire recording is composed by 21 ramps. One possible recruitment order is represented by the first column of the table which appears 2 times on 21 ramps, the second possible recruitment order was found 7 times on 21 ramps, ...

RecOrder1	**RecOrder2**	**RecOrder3**	**RecOrder4**	**RecOrder5**	**RecOrder6**
20	20	20	20	20	20
23	23	6	6	14	14
6	14	23	14	23	6
14	6	14	23	6	23
2/21	7/21	1/21	4/21	4/21	3/21

Table 4.2. Recruitment order/sequence for subject 1 during medium contractions (30%MVC/s).

It is worth noting that the numbers used to represent the motor unit must be read not in terms of motor unit recruitment but as simple output of the decomposition procedure (e.g. see Table 5.4: in the first row, the first MU indicated as '20' means that it is the twentieth motor unit found by the CKC algorithm).

Finally, the average discharge rate (DR) for each single motor neuron and across the trials at the different speeds was calculated. The inter-spike interval (ISI) was calculated as the inverse of the time (ms) elapsed between each pair of consecutive spikes (Sartori *et al.*, 2017):

$$ISI_i = \frac{1}{tc_{(k+1)} - tc_{(k)}} \tag{4.5}$$

where tc_k is the discharge time of the k^{th} spike for the i^{th} motor neuron. Thus, for each MUs a vector containing the ISIs was stored to evaluate the mean discharge rate. To provide a direct measure of the average firing of the active motor neurons, the vectors containing the ISI were smoothed using a moving average window of 500 samples (Sartori *et al.*, 2017).

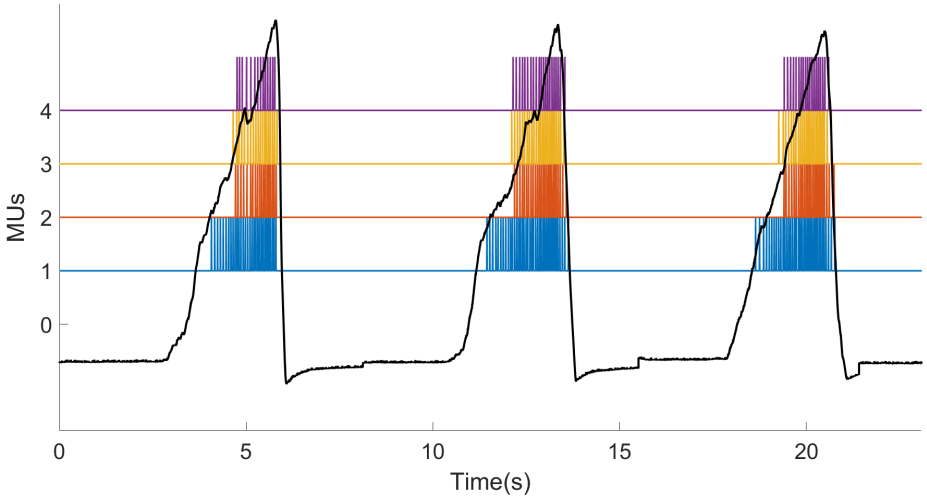

(a)

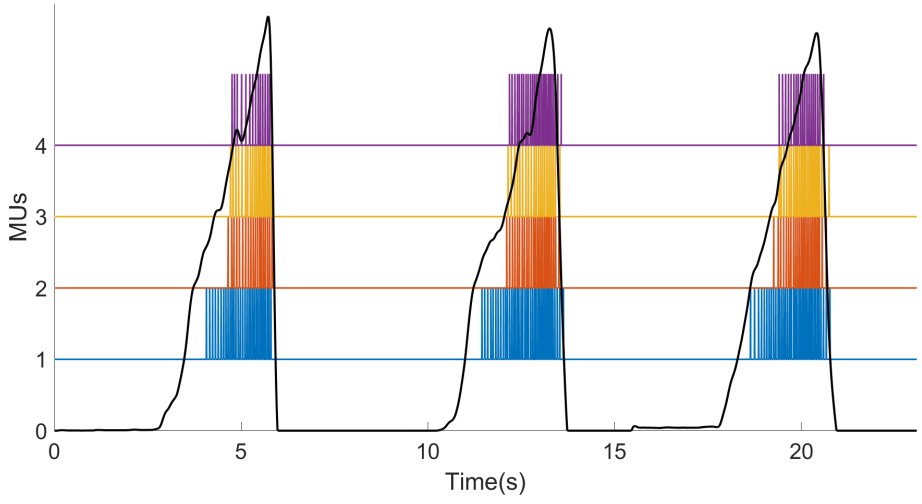

(b)

Figure 4.4. Discharge patterns considering three ramp contractions performed at 20%MV/s. Here, 4 MUs are shown (result obtained from the tracking). In (a) MUs are not organized in their recruitment order, while in (b) the same motor units are shown ordered according to their relative recruitment threshold.

Chapter 5

Results and discussion of the EMG signal decomposition

5.1 Analysis of the CKC inspector results

Starting from the information given by the *CKC inspector* output, all graphic results were plot in MATLAB to observe the MUs properties across the three different speed of the contraction. On average the algorithm detected more than 10 MUs per recording (see Table 5.1). Each outcome is presented in three different ways:

1. innervation pulse train (IPT) (see Fig. 5.1(b)), 5.2(b), 5.3(b)) which displays the train of MU discharge times estimated by the decomposition technique. Each coloured dot represents a MUAP arrival at the time indicated on the horizontal coordinate (ms). The right vertical coordinate represents the instantaneous discharge rates in pulses per second (pps). The left vertical coordinate reports the number of MUs identified by the algorithm.

2. Smoothed MU discharge rates (see Fig. 5.1(c)), 5.2(c), 5.3(c)) that is the mean firing rate of the different MUs. Each plots is represented by coloured lines. The mean firing rate values are reported in pps on the left vertical coordinate while the horizontal coordinate represents the time of the contraction. This kind of plot allows to study the relationships among different motor units.

3. the motor unit action potential trains (MUAPTs) represented as delta functions (see Fig. 5.1(a)), 5.2(a), 5.3(a)) measured in units of time. Each horizontal strips correspond represents an impulse, that that is a different MUAPT.

In each plot, the grey continuous line represents the output force (N) (see Fig. 5.1, see Fig. 5.2 and see Fig. 5.3). For clarity reason, only the first three ramp contractions are given for each different level of force and one subject is taken as representative.

Subject ID	Slow 1s	Medium 2s	Fast 3s
1	11	23	9
2	13	22	12
3	17	10	15
4	16	16	21
5	13	14	17
6	7	9	5
7	4	5	6

Table 5.1. Number of decomposed motor units per subject.

Each plot is useful to identify the decomposition errors. For example in Fig. 5.1(b)), 5.2(b), 5.3(b) the presence of isolated dots out of range, that is abnormally long or short pulse interval between two occurrences, are indicative of a missed detection or of a misclassification. In this case, the visual inspection help to reconstruct the expected pattern based on the previous events observed in all the monitored motor units. In addition, the representations results may be useful to understand if the mean firing rate is in its physiological ranges that range between 20-50 pulse per second (pps) (see Fig. 5.1(c), 5.2(c), 5.3(c)). In particular, by plotting the results for different speed of the contraction, different firing rates modulation are represented. For the ramp contraction performed at 20%MVC/s (slow speed of the contraction) and 30%MVC/s (medium speed of the contraction), the mean firing rates varies between 15–30 pps (see Fig. 5.1(c), 5.2(c)). On the contrary, the smoothed instantaneous discharge rates for the ramp contraction performed at 60%MVC/s (fast speed of the contraction) ranging from 40–60 pps (see Fig. 5.3(c)).

Two other differences are emphasized considering the slow and the fast speed of the contraction. One of them regards the discharge rates: during rapid ankle dorsi-flexion movement there is a high initial discharge rate that declines progressively (see Fig. 5.3(b), 5.3(c)) with respect to the contraction performed at slow speed (see Fig. 5.1(b), 5.1(c)) where the MUs fire progressively. The second observation regards the number of spike (see Fig. 5.3(a)): during the rapid movements (60%MVC/s) the activated MUs fire less ($\sim$ 1–20 times) with respect to the slow movements (>40 times) (see Fig. 5.1(a)) (Van Cutsem & Duchateau, 2005; Van Cutsem *et al.*, 1998). These observations underscore both the difference in MU activation pattern comparing slow and rapid contractions and they show the different strategies actuated by the CNS to obtain a certain level of force. Thus, the EMG signal decomposition may be beneficial in research activities interested in motor unit properties and behaviour and in clinicians studies to asses the state of the muscles (Mambrito & De Luca, 1984).

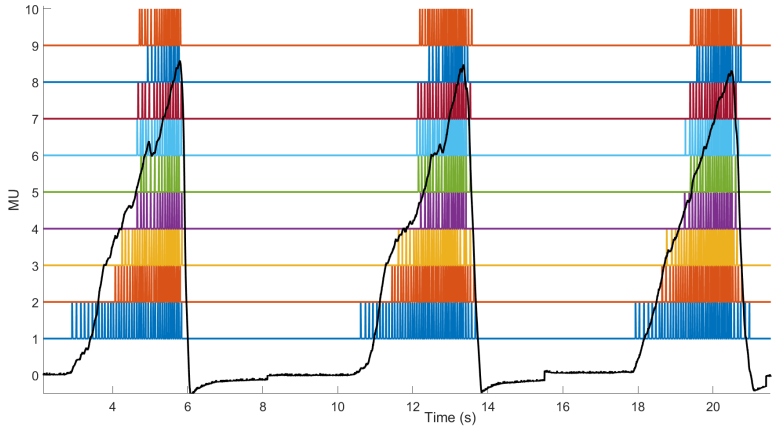

(a)

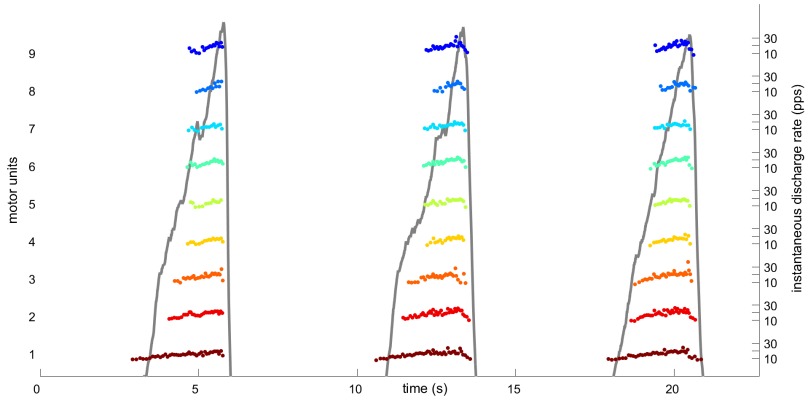

(b)

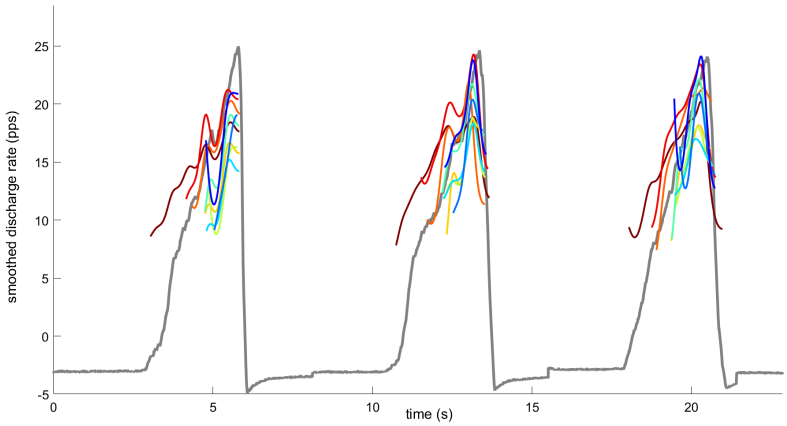

(c)

Figure 5.1. Speed of the contraction at 20%MVC/s.

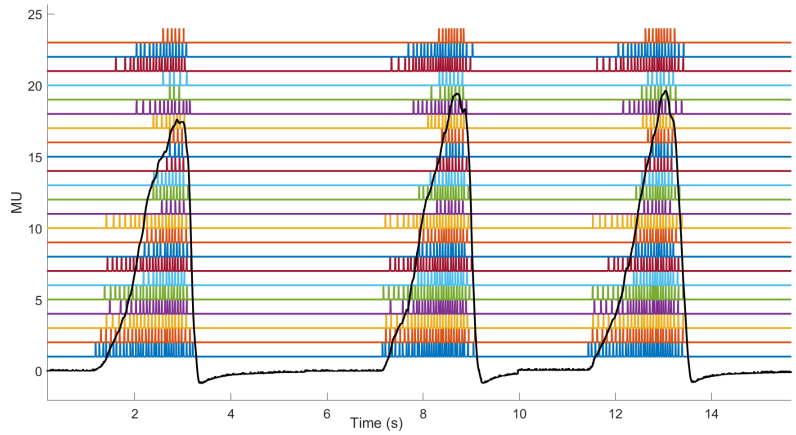

(a)

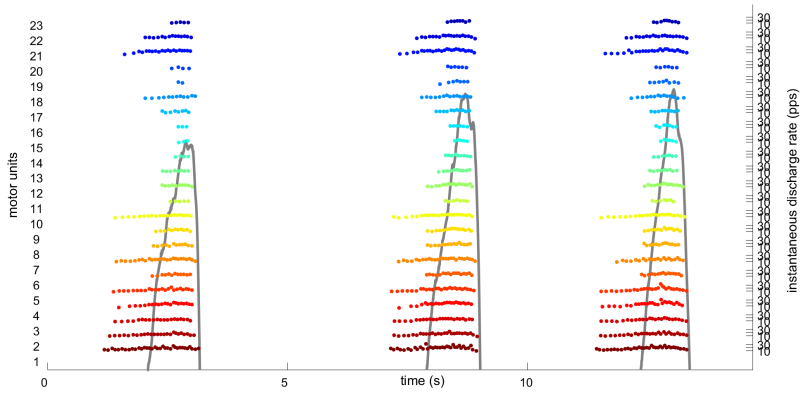

(b)

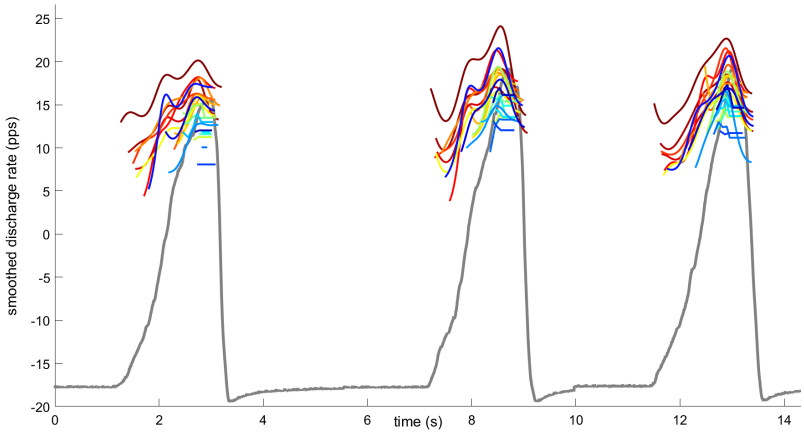

(c)

Figure 5.2. Speed of the contraction at 30%MVC/s.

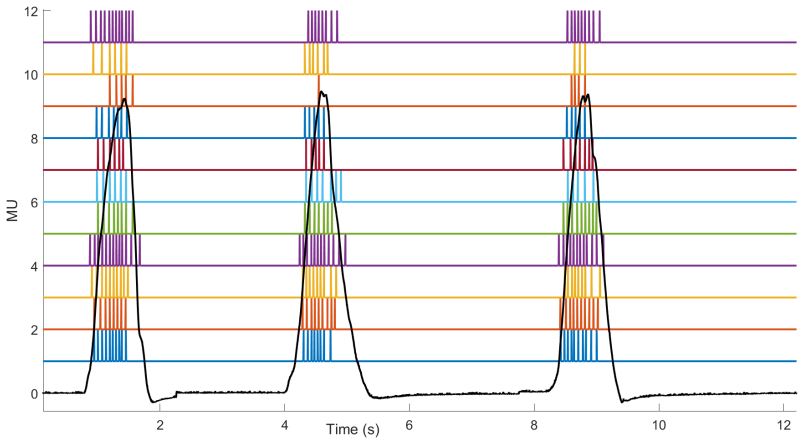

(a)

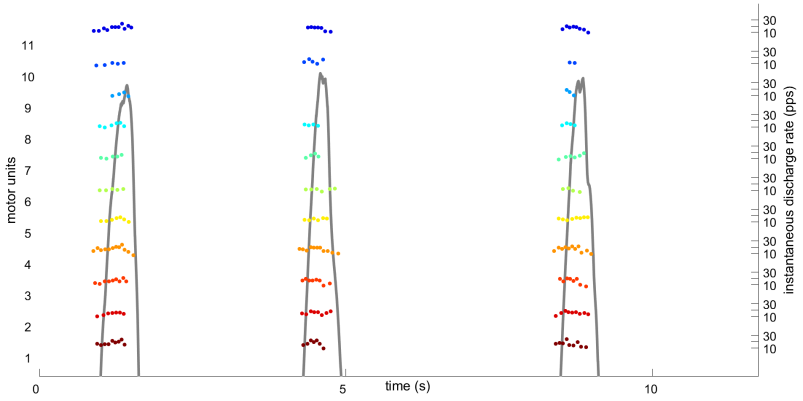

(b)

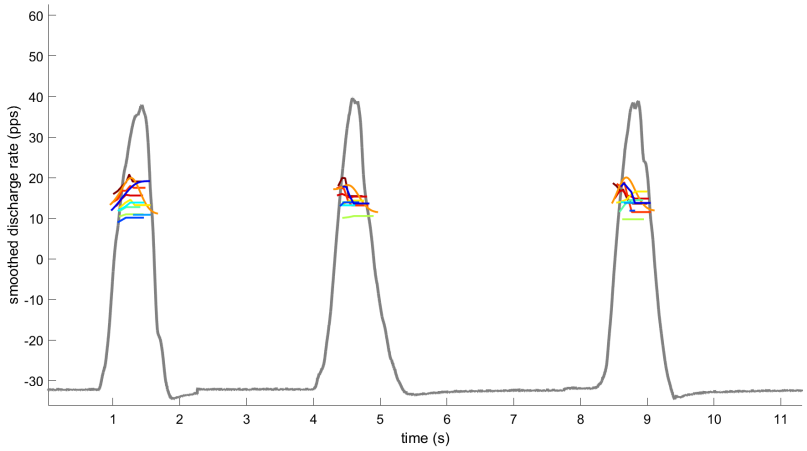

(c)

Figure 5.3. Speed of the contraction at 60%MVC/s.

5.2 MU recruitment and firing rate properties

The idea to follow the same MU using the spike triggered averaging technique first and the maximum of the correlation between the MUAP shapes over different recordings, allows to verify the decomposition accuracy. Indeed, the HDEMG contains the activity of many MUs, thus the possibility to monitor the same MUS over different condition shows that all of the discharges identified are correctly. This is demonstrated by the decomposition templates (see Fig. 4.2 in Chap. 4) and by the high mean correlation value (see Table 4.1 in Chapter 4). The results obtained by the tracking of MUs support the validity of the surface EMG decomposition technique. Is worth to note that matching the MUs across different trail is appropriate for the conditions that were tested in this project, that is the isometric contraction. Indeed, during dynamic conditions the MUAP waveform could change, thus the feasibility of the tracking may not be reliable (Kapelner *et al.*, 2018).

The recruitment orders, force threshold and mean DRs are investigated using the tracked MUs. The MUs recruitment orders are investigated in terms of permutations (see Tables 5.2, 5.3 and 5.4 the results of the permutations for one representative subject). The results obtained show a preferential recruitment order across the different trials. This is demonstrated by the ratio between the number of times that a certain order appears and the total number of ramps (for example, as reported in Table 5.2, for subject 1 at slow contraction velocity, the second recruitment order is mostly represented, indeed it appears 12 times on 19 ramps). In addition, it is possible to note that the different recruitment order usually vary for one/two positions (see Table 5.2 where the two recruitment orders are different for the position held by MU_2 and MU_6). Three possible reasons may justify this variability of motor unit recruitment sequence:

1. the imperfect automatic decomposition in the spike identification due to the noise (Farina & Enoka, 2011);

2. the manual processing;

3. the close recruitment thresholds between motor units (see Fig. 5.4 and Fig. 5.5).

RecOrder1	RecOrder2
5	5
9	9
2	6
6	2
7/19	12/19

Table 5.2. Recruitment order for subject 1 during slow contractions (20%MVC/s).

RecOrder1	RecOrder2	RecOrder3	RecOrder4	RecOrder5	RecOrder6	RecOrder7
6	6	6	6	6	4	5
3	3	4	5	5	5	6
4	5	3	3	4	6	3
5	4	5	4	3	3	4
5/29	5/29	1/29	10/29	5/29	2/29	1/29

Table 5.3. Recruitment order for subject 1 during fast contractions (60%MVC/s).

RecOrder1	RecOrder2	RecOrder3	RecOrder4	RecOrder5	RecOrder6
20	20	20	20	20	20
23	23	6	6	14	14
6	14	23	14	23	6
14	6	14	23	6	23
2/21	7/21	1/21	4/21	4/21	3/21

Table 5.4. Recruitment order for subject 1 during medium contractions (30%MVC/s).

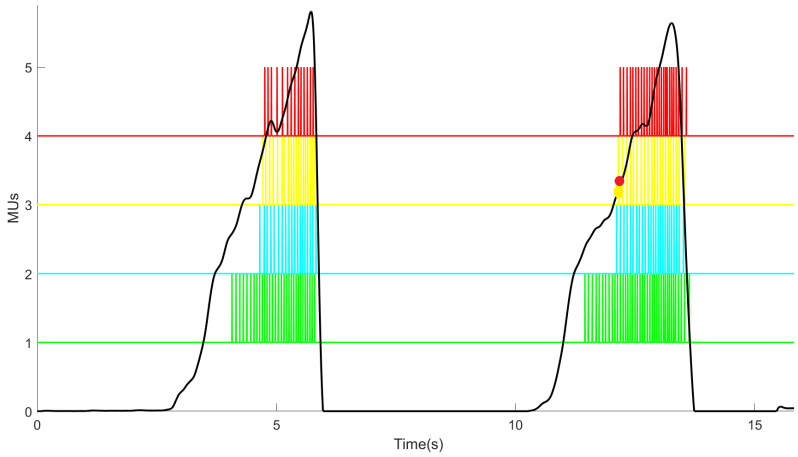

(a)

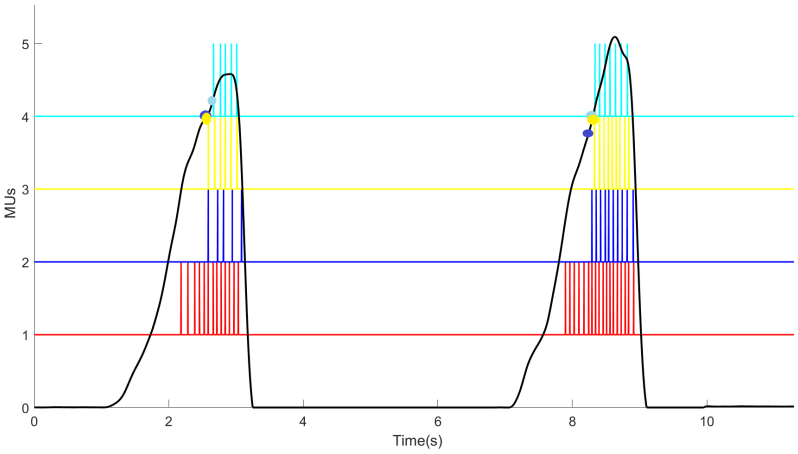

(b)

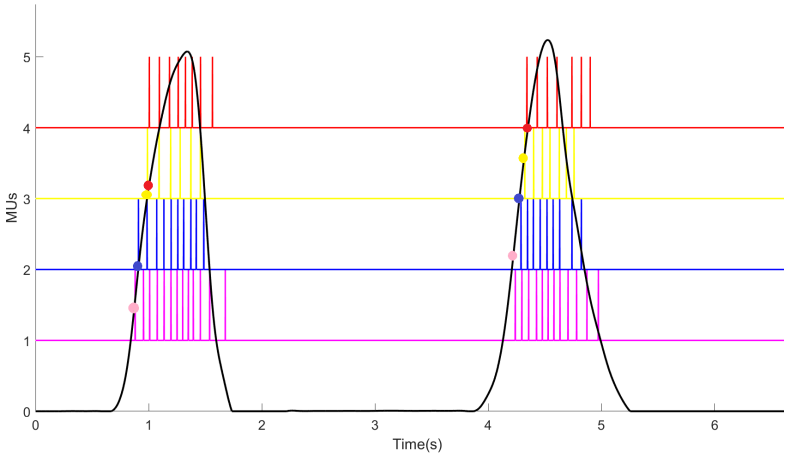

(c)

Figure 5.4. 20%MVC/s in (a), 30%MVC/s in (b) and 60%MVC/s in (c). Results for one representative subject.

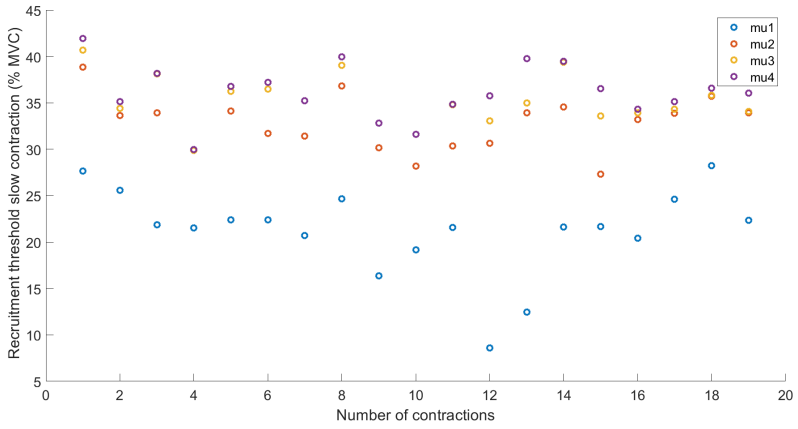

(a)

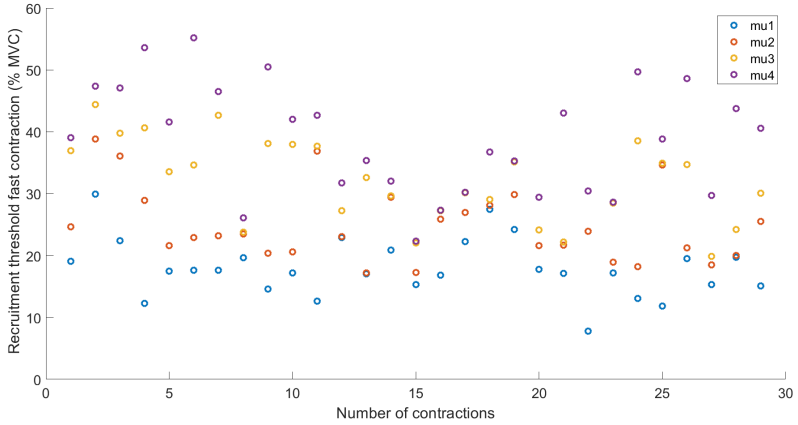

(b)

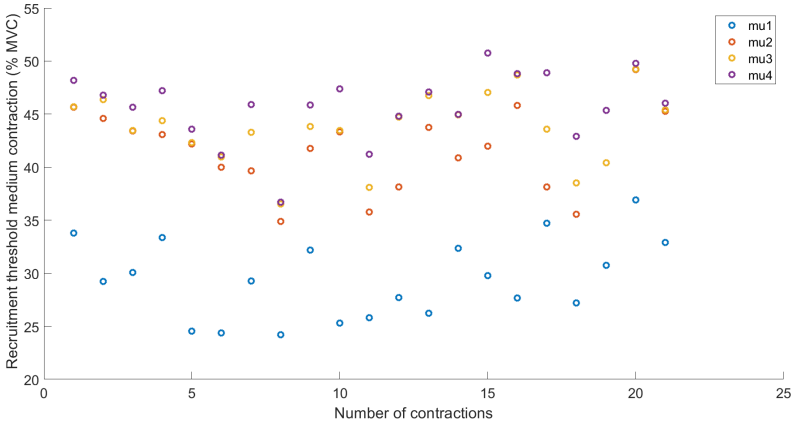

(c)

Figure 5.5. Spread of the recruitment force thresholds for all MUs. Results for one representative subject.

The percentage of force at which motor units were recruited provides information regarding motor unit recruitment in contractions of different speed (see Table 5.5). We observed that MUs recruitment threshold decreased with the increase in the speed of contraction and our findings were in agreement with previous reports (Masakado *et al.*, 1995).

Subject ID	**Slow 3s**	**Fast 1s**
S1	31%MVC	28%MVC
S2	33%MVC	31%MVC
S3	25%MVC	31%MVC
S4	36%MVC	30%MVC
S5	29%MVC	28%MVC
S6	31%MVC	28%MVC
S7	31%MVC	31%MVC

Table 5.5. Average motor unit recruitment threshold (%MVC) per subject. Only 2 participants out of 7 showed an higher recruitment threshold in fast compared to slow contractions (highlighted).

The results achieved for the mean DRs modulations (see Fig. 5.6) are in accordance to the "onion skin" theory (De Luca & Hostage, 2010). Indeed, the mean DR of the earlier recruited MUs (low threshold) was always higher than those of the high threshold motor units (Masakado *et al.*, 1995). According to Henneman's size principle, the latest recruited MUs are more fatigable; thus considering their lower firing rate some benefits may be to help to maintain a sustained contraction limiting fatigue, to contribute in finer muscle force control or to provide a greater force if it is needed (De Luca & Contessa, 2012). Furthermore, the lower firing rate might depend on the fact that the later recruited MUs are closer to the end of the contraction, thus they receive a smaller excitation drive and the neural commands may diminish (Hu *et al.*, 2014).

Tracking the individual motor units over time and over different conditions, can provide observations regards the MUs properties. In particular, it is possible to observe the behaviour of the same MU when it is recruited for slow and high level of force. Indeed, the different properties shown (i.e. the mean discharge rates) illustrate how the CNS may recruit the same MU in different speed of the contraction, but it modulates and changes both the MUs discharge rates and the threshold of the force recruitment.

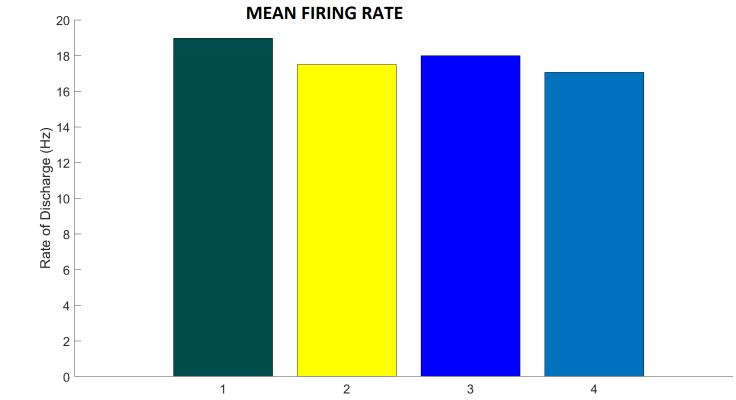

(a)

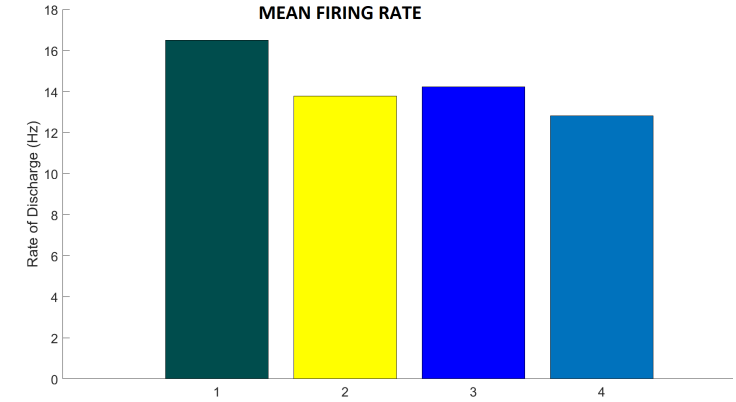

(b)

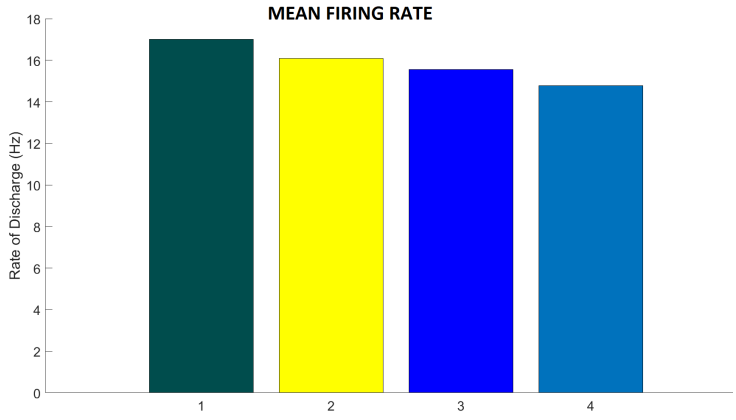

(c)

Figure 5.6. Mean firing rate across the trials considering the three speed of the contraction. In (a) slow speed, in (b) medium speed and in (c) fast speed of the contraction. Results for one representative subject. The MUs are indicated as 1, 2, 3 and 4.

Chapter 6

Contractile impulse estimation

Based on the results obtained in Chapter 5 regards the force control, in this chapter are designed different force estimators using two models. The estimators are designed considering all the MUs identified by the decomposition algorithm (see Table 5.1, Chapter 5). This choose depends by two main reason:

1. a priori we do not know how many and which MUs will be recruited in the muscle contraction, thus we can not used only the tracked MUs;

2. all the information extracted by the decomposition are an useful mean to infer the neural drive to the muscle, thus to obtained a good force estimator.

In order to estimate the force expressed by the muscle during the ankle dorsiflexion the linear regressions were designed. Starting from the EMG signal, two different approaches have been investigated: the first based on the summation of discrete single motor neuron spike trains (neural drive), the second based on the EMG envelope (global EMG feature) extracted from the HDEMG. Both the regressions were done considering a time domain feature extracted from the recording force, e.g. the contractile impulse (IC). This was calculated as the integral of the force along time. Thus both for the EMG envelope and the neural drive (ND), the regressions were evaluated with the integral of the signals in each contraction, instead of the signal itself. The whole process is graphically summarized in Fig. 6.1 and described in detail in the next sections. In particular, the three signals were processed separately, then the two regressions were evaluated and their performances were compared. The regressions were determined both considering the measured force for each different speed of the contraction (three different regressions) and the global force resulting by their grouping. In this way, the two different regression models allowed to study the single effects and the total one in the force estimation. The performances obtained in the IC estimation from the ND and EMG model-based, were compared with the aim to find the best estimator. In this work, the IC was intended as a parameter to estimate the ability of a subject

to generate his maximal force considering different conditions, as the variation of the speed during limb movements. The integral of the ND represents the changes in the motor neuron discharge rates and/or in the MU recruitments during a certain activity, while, the integral of the EMG envelope reflects the changes in its amplitude.

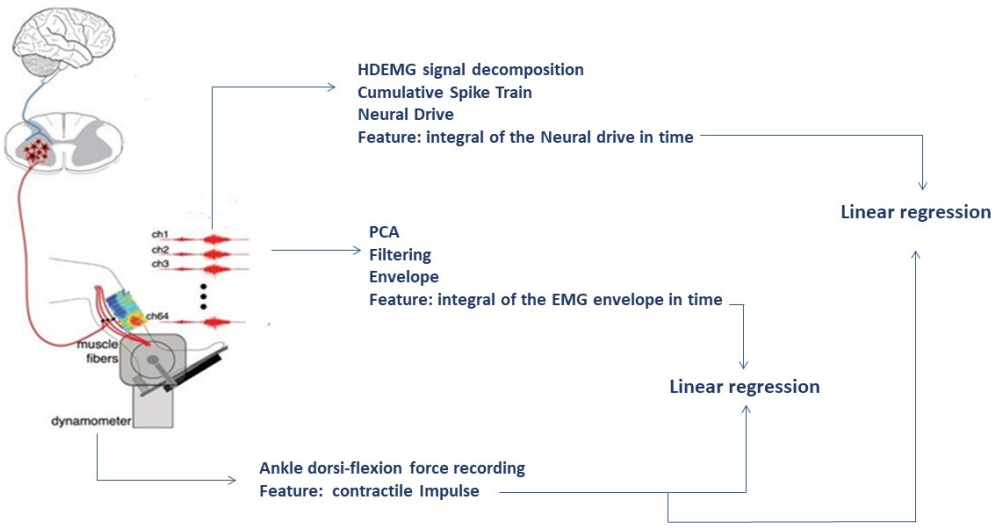

Figure 6.1. Block diagram of the processing steps for each of the three signal: force, emg envelope and ND. Figure in the left of the block diagram is adapted from (Sartori *et al.*, 2017)

6.1 Motor neuron decoding and Neural Drive extraction

The information extracted by the convolutive blind source separation algorithm (described in Chapter 3) provides the motor neuron activity in the time domain (individual spike discharge trains). To differentiate the periods of motor neurons activity from no activity, each single spike trains was converted in a binary sequence of zeros and ones. In particular, to each sample was assigned 0 or 1 depending on whether or not the sample marked an action potential. Then, the cumulative spike train (CST), was evaluated as the sum of the single spike trains for all motor units (see Fig. 6.3). The CST is obtained by combining together the single discrete spike trains, where each spike in it is marked as 1; in each time instant the CST is the sum of motor units that are simultaneously active (see Eq. 6.1). The relation

between the input received by each motor neuron j-th in a pool N and the resulting value of cumulative at time i-th is modelled as:

$$cst(i) = \sum_{j=1}^{N} MU_j(i) \tag{6.1}$$

where $MU_j(i)$ assumes 0 or 1 depending on whether or not the MU j^{th} at time i^{th} was active. In this way, the CST is a discrete dimensionless signal in time. The resulting CST is a direct estimation of the total activities of motor neurons that share a common input, defined as *effective* neural drive (Farina *et al.*, 2014). Since the motor unit discharge timings can be mathematically described as a set of delta functions, the resulting CST is an impulse function too, with its maximum value equal to the sum of all identified motor units (see Fig. 6.4(a)).

To limit its value in a range between 0 and 1, the CST was normalized on the number of MUs that could fire at the same time. In this way, the CST indicates the percentage of MUs concurrently active. After the normalization, the discrete CST was filtered with low-pass filter at 2 Hz (Butterworth, 6rd order) to obtain a continuous signal along the time and evaluate the integral on a specific interval (see Fig. 6.4(b)). This filter was realized using the MATLAB function *Butter* in order to find the transfer function coefficients (*B,A*). The filtering is executed using the MATLAB function *filtfilt*) (see Fig. 6.1).

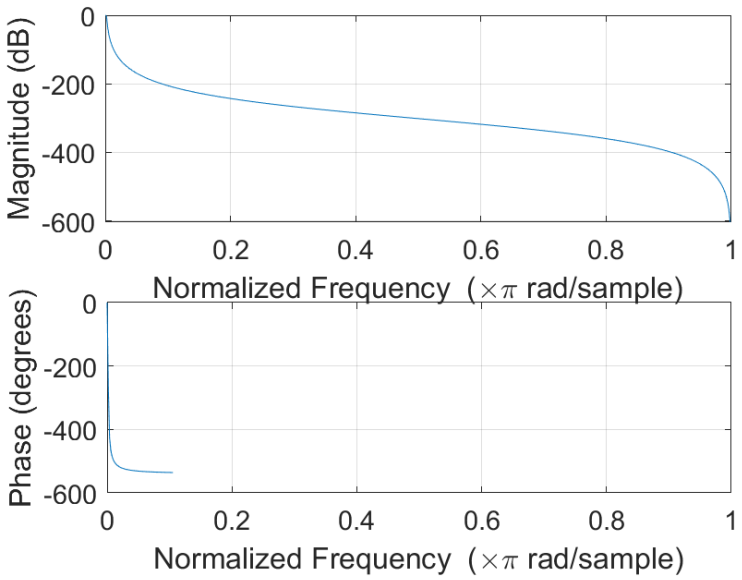

Figure 6.2. Mask of the low-pass filter. The cut off frequencies is normalized between 0 and 1, where 1 corresponds to the Nyquist rate-half the sample rate.

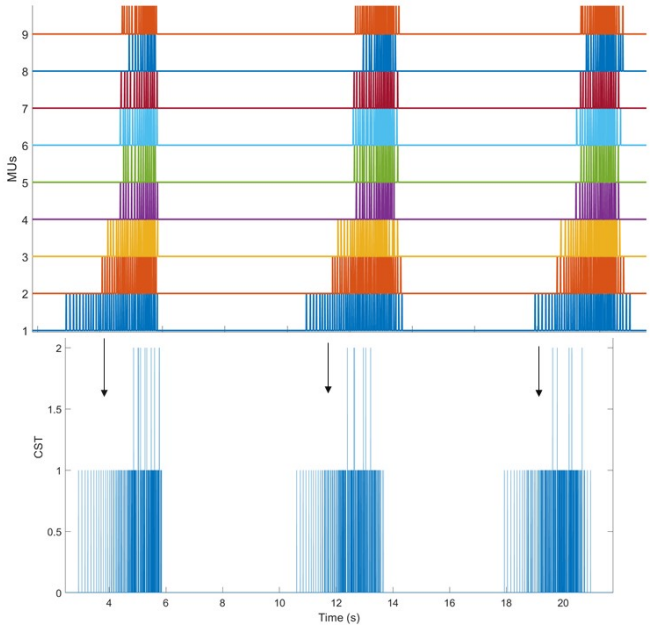

Figure 6.3. The process to obtain the cumulative spike train (CST).

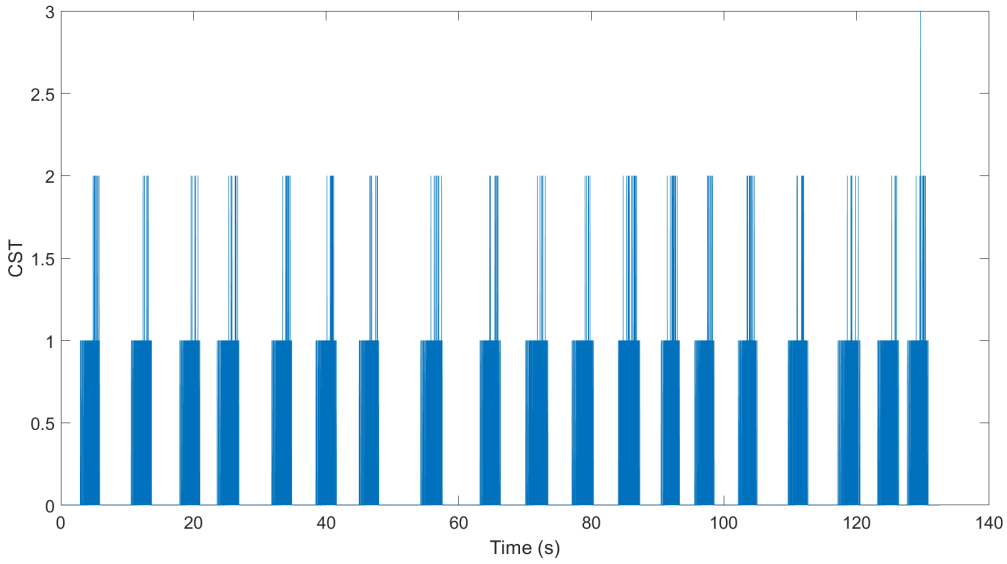

(a)

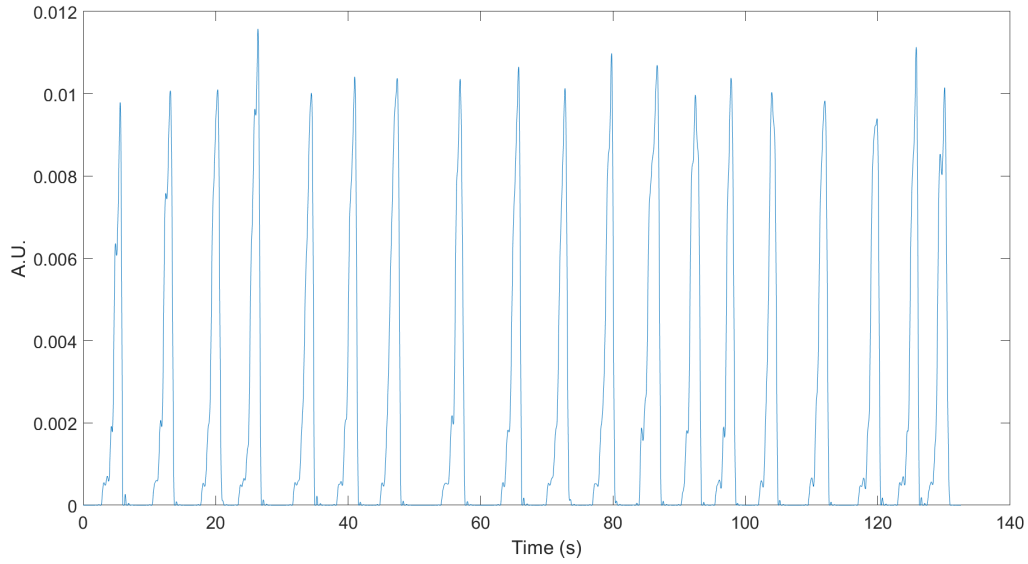

(b)

Figure 6.4. The cumulative spike train (CST) in (a) and its continuos-smooted version. Ankle dorsi-flexion performed at 20%MVC/s.

6.2 Global EMG envelope extraction

All the HD-EMG signals recordings described in Chapter 3 were performed in monopolar derivation. An additional filtering step is added to the interferent HD-EMGs. Indeed, the sEMG were band filter by the hardware filter at 10-500 Hz (see Chapter 3). In particular, the signals were band-pass filtered using a zero-phase filter (Butterworth, 3rd order) with cut-off frequencies 20 Hz and 500 Hz (see Fig. 6.2). This filter was realized using the MATLAB function *Butter* in order to find the transfer function coefficients (*BEMG,AEMG*). The filtering is executed using the MATLAB function *filtfilt*) that allows to avoid the phase distortion and the filter delay. The choice of this bandwidth is in according with Hakonen *et al.* (2015). Indeed, the low frequency cut-off removes the movement artefact component (bandwidth 5-30 Hz), while the high frequency cut-off removes harmonics components higher than 500 Hz. According to De Luca *et al.* (2010), most of the energy of the EMG signal is limited between 400–500 Hz.

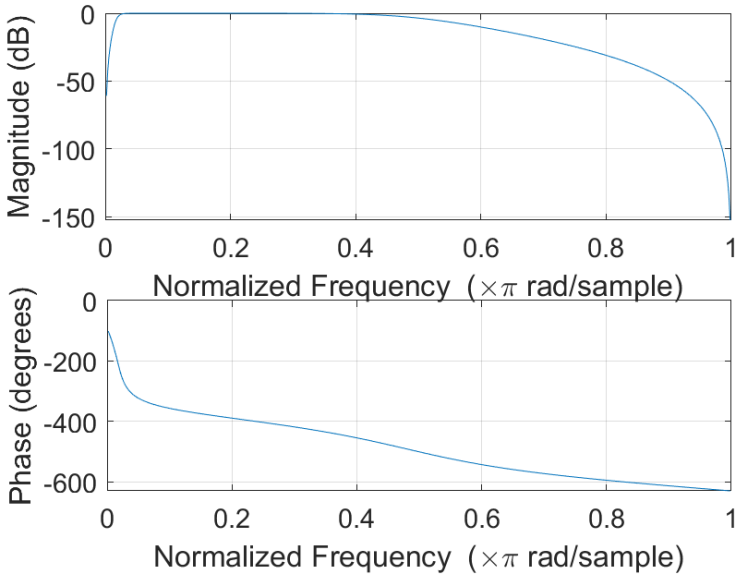

Figure 6.5. Mask of the band-pass filter. The cut off frequencies is normalized between 0 and 1, where 1 corresponds to the Nyquist rate-half the sample rate.

Due to the high dimensionality of the HD-EMG, the signals may contains redundant information (Staudenmann *et al.*, 2006), thus the Principal Component Analysis (PCA) was used to extract the most representative part. In this way, the principal component that identified the common temporal patterns across large datasets (HDEMG) (Naik *et al.*, 2016) was extracted using MATLAB function *PCA*. This function returns the principal component coefficients and the percentage of the total variance explained by each principal component. In this work, the

resulting mean principal components retained respectively 75,42% 72,57% 71,57% of the original variance for fast, medium and slow speed of the contraction. The resulting signal was rectified and its linear envelope was extracted with a low-pass filter (Butterworth second order) with cut-off frequencies at 2 Hz. Then, the amplitude offset of the resulting signal was removed to achieve zero mean and the EMG amplitude was converted to mV (see Fig. 6.6).

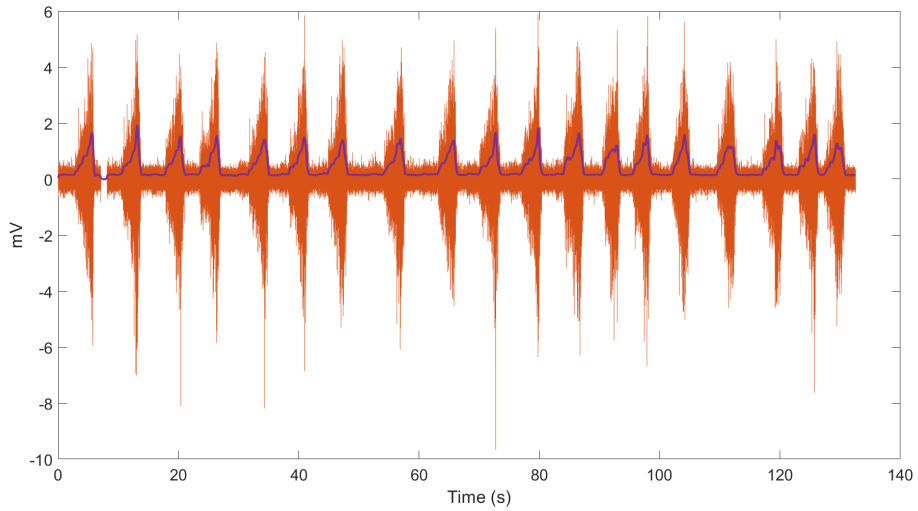

(a)

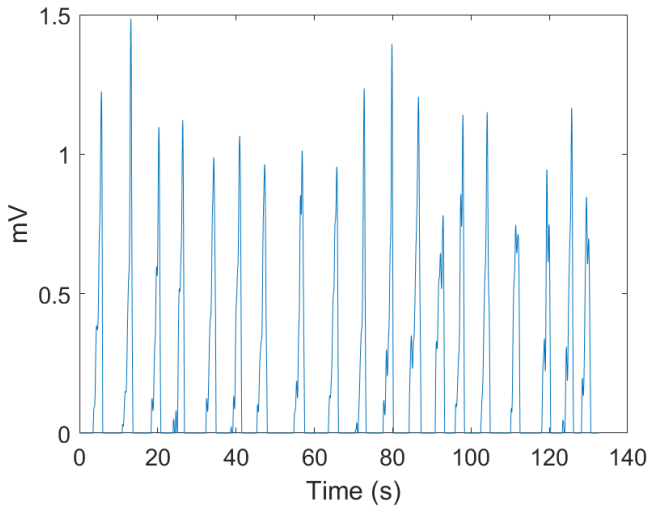

(b)

Figure 6.6. Trend of raw EMG (orange signal) and its envelope (violet signal) in (a). EMG envelope in (b). Recording performed at 20%MVC/s.

6.3 Muscular activity onset detection

Before evaluating the regressions, the duration of EMG activity was defined. For this reason, it was necessary to determine the specific time instant that marked the beginning and the end of the EMG activity. To detect the on and off timing of the muscle, a threshold-based method (Hodges & Bui, 1996) was applied. According to this method, the onset (and offset) of muscle activity was define as the first point when the EMG signal exceeded T_{noise}:

$$T_{noise} = \mu + h\sigma \tag{6.2}$$

where μ and σ represent the mean and the standard deviation of the noise signal respectively, while h is a parameter to defined the threshold level and it was set to 2 (Tedroff *et al.*, 2006). Thus, it was necessary to defined a noise source to estimate the mean μ and the standard deviation σ. Since from the experimental protocol, each isometric ankle dorsi-flexion was interspersed with 5s of resting periods, it is possible to consider in this time interval, no muscular activity. Due to the neuromechanical delay (NMD), defined as the time delay between the rise time of the motor unit action potentials and the respective force output (Del Vecchio *et al.*, 2018), the cross correlation between the ND and the force was calculated using the MATLAB function *xcorr*. This function returns a vector with the lags at which the correlations are computed. Thus the maximum lag is found to aligned the two signals. In this way, the force and the ND were aligned with respect to their time delay because at that value the cross-correlation of them is maximum. On average, the cross correlation was equal to 95% considering all subjects and all speeds of the contraction. For this reason, it is possible to consider the ND as a reliable indicator of the muscle activation, thus the onset of the EMG activity on the ND were evaluated on it. The ND calculated for each speed of the contractions was plotted and a manual selection of a time interval with no EMG activity, was performed. In these, the time interval between two ramp contractions was defined as the noise interval. The results of the onset and offset detection are shown in Fig. 6.7.

6.4 Linear regressions

The shape similarity shown in Fig. 6.7 between the force (orange lines) and the ND (red lines) generated suggested a high relationship between the two signals. According to the experimental protocol described in Chapter 3, the participants in the experiment performed several ramp contractions ($\sim$ 25), at three different speeds, with a ramp duration of 3s (slow speed), 2s (medium speed), and 1s (high speed). Thanks to this, it was possible to observe the manifestation of the muscle strength in different time intervals. In these interval the ICs were calculated as

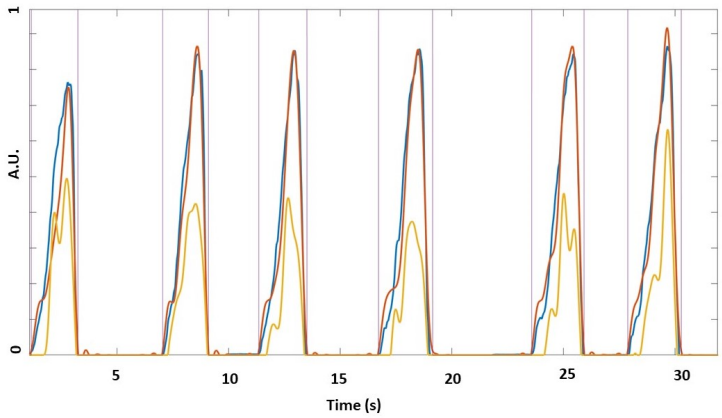

Figure 6.7. Results of onset-offset detection using the threshold-based method. Six ramp contractions, normalized to their maximum value, are illustrated: in blue the EMG envelope, in red the neural drive and in orange the recorded ankle dorsiflexion force. In violet the windows of the onset/offset muscular activity.

the area under the measured force signal, i.e. the time integral of the force. In order to investigate the relationship between the IC and both the ND and the EMG, the integrals of the signals in each contraction were calculated. This was done considering the three single linear regressions (SLR) corresponding to each speed of the contraction (see Fig. 6.9) and one single global regression (GLR), where the three forces were put together (see Fig. 6.10). This double analysis, the single regressions and the global regression, are due to the fact that in the event of implementing a controller able to control the force, such as in myoelectric prosthesis, the speed of the contraction is not known a priori. It means that, it is not possible to decide what type of regressor works better among the three available. For this reason, a global regressor is designed and its performance is tested. It is clear that in this way, we are going to lose important informations on our system (velocity contraction), which may provide a more accurate control. On the other hand, a global regressor would be suitable for more general situations and representing a fair trade-off among the three conditions. To obtain the polynomial coefficients for the regressions the MATLAB function *polyfit* was used. These coefficients were are used in a second function *polyval* to evaluate the linear regression.

Finally, considering the case of using this force estimation for a myolectric control, an important drawback rises up: the time delay. In fact, according to the regressor presented above, the force estimation needs at least 1 second (considering the fast contraction) of contraction for evaluating the respective force. This delay severely increases for medium and slow contractions, up to 3 seconds. An efficient solution to this is to consider a time window (Farrell & Weir, 2008). In this work, a time window of 200 ms was used. Also for this solution, the analysis was conducted

formulating both a velocity custom linear regressor (see Fig. 7.7) and a global one (see Fig. 7.9).

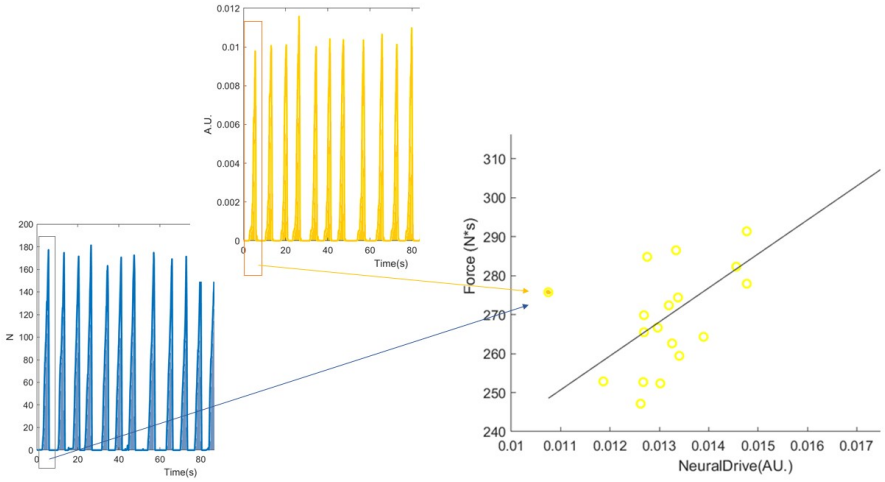

Figure 6.8. An example of the regressions designed. The coordinates of each dot on the graph are represented by the time integral calculated under the force curve and the curve of the neural drive (the same description for the EMG envelope). Here, the ramp of 3s (slow speed) is shown.

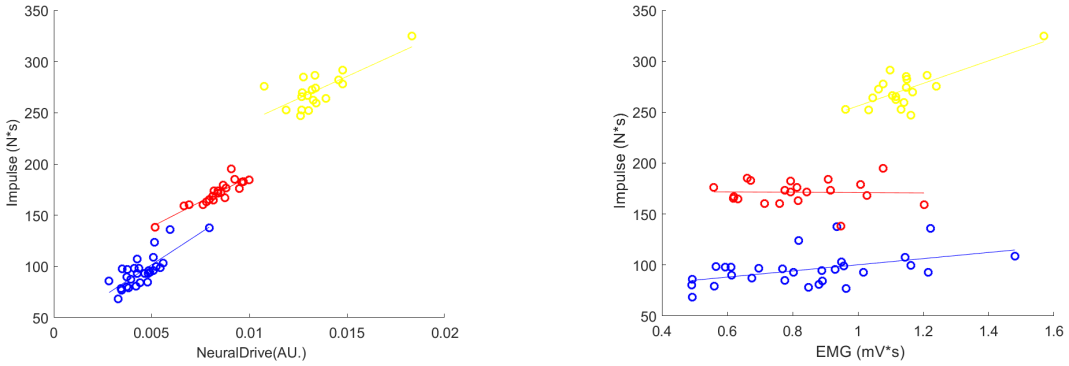

(a) (b)

Figure 6.9. In (a) the ND model-based estimator, in (b) the EMG envelope model-based estimator. Two examples of the regressions used to estimate the contractile impulse for one representative subject. In (a) and (b) the three single regressions are depicted in different colours: slow speed in yellow, medium speed in red and fast speed in blue.

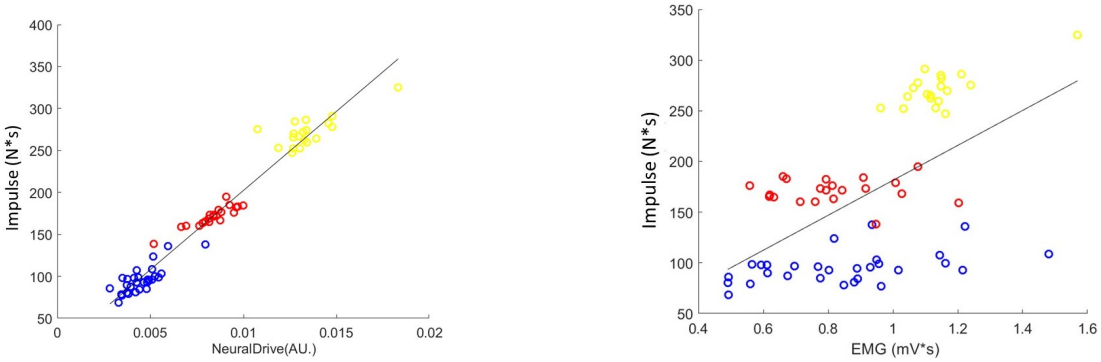

(a) (b)

Figure 6.10. Global linear regressor. In (a) ND model-based estimator, in (b) EMG envelope model-based estimator.

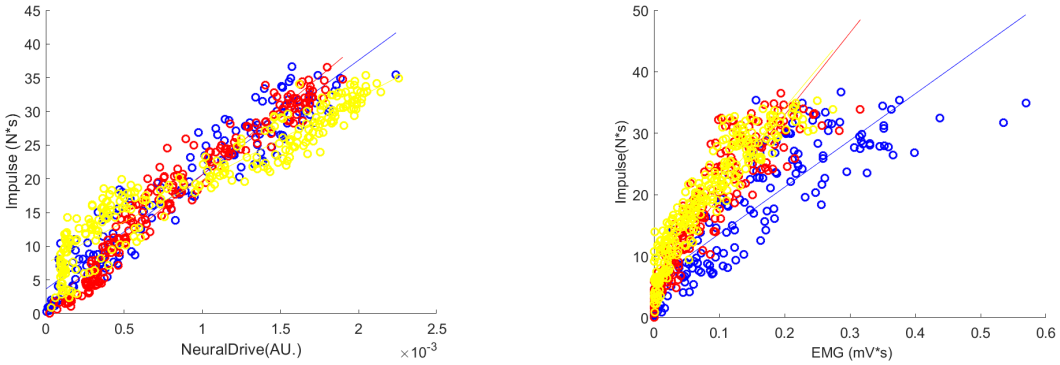

(a) (b)

Figure 6.11. In (a) ND model-based estimator, in (b) EMG envelope model-based estimator. Two examples of the regressions used to estimate the contractile impulse for one representative subject considering a moving window of 200ms. In (a) and (b) the three single regressions are depicted in different colours: slow speed in yellow, medium speed in red and fast speed in blue.

6.5 Statistical analysis

To quantify the performance of the regressions, the R^2 value has been use. R^2 was defined as:

$$R^2 = 1 - \frac{SSE}{SST} = 1 - \frac{\sum_{i=1}^{n}(y_i - f_i)^2}{\sum_{i=1}^{n}(y_i - \hat{y})^2} \tag{6.3}$$

SSE (sum of squared errors of prediction) is the sum of the squared residuals and SST (total sum of squares) is the sum of the squared residual from the mean observed value ($\hat{y}$) and it is proportional to the variance. The residuals are calculated

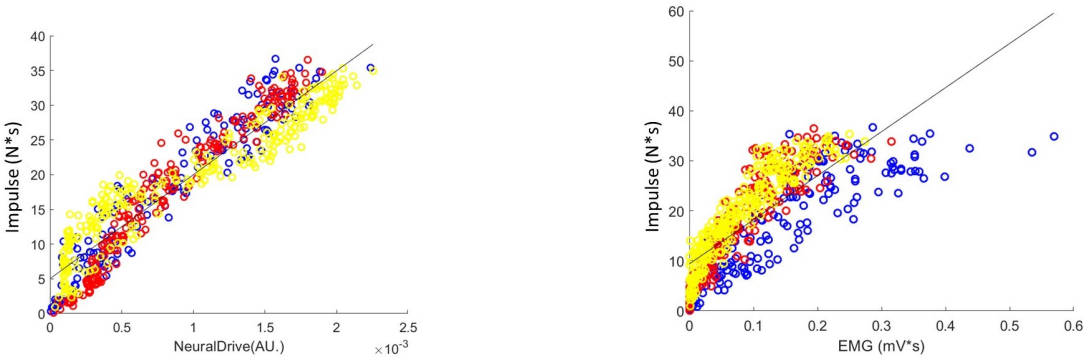

(a) (b)

Figure 6.12. Global linear regressor. In (a) ND model-based, in (b)EMG envelope model-based.

as the difference between the force value measured during each task of the ankle dorsi-flexion (y), and the force estimated with the specific linear regressor (f).

Since the population mean and standard deviation were unknown, the Lilliefors test was performed to assess if the R^2 values came from a standard normal distribution. Once the normality has been verify, a parametric paired t- test was used to statistically compared R^2 values. The significance level for all statistical comparisons was set at $p\ value < 0.05$. The statistical analysis was performed to asses the statistical difference between all R^2 values obtained from the 7 subjects. In particular, between the ND model-based linear regressor and the EMG envelope model-based linear regressor the R^2 values statistically compared were:

1. ${}^{ND_{SLR}}_{w}R^2_{s/m/f}$ and ${}^{EMG_{SLR}}_{w}R^2_{s/m/f}$ that are the results of the single force estimations. The superscripts *SLR*, *ND* or *EMG* indicate the SLR models considering the ND and the EMG model-based. Since the regressions are designed considering both the whole contraction and the moving window, the subscript w indicates the whole contraction while *f*, *m* and *s* indicate respectively fast, medium and slow.

2. ${}^{ND_{SLR}}_{mw}R^2_{s/m/f}$ and ${}^{EMG_{SLR}}_{mw}R^2_{s/m/f}$ that are the results of the single force estimations considering the moving window (the subscript w). The superscripts *SLR*, *ND* and *EMG* indicate the SLR models considering the ND and the EMG model-based. Since the regressions are designed considering both the whole contraction and the moving window, the subscript mw indicates the moving window. The subscripts *f*, *m* and *s* indicate respectively fast, medium and slow.

3. ${}^{ND}_{w}R^2_g$ and ${}^{EMG}_{w}R^2_g$ are the results of the global force estimation. The subscript g indicates the GLR model for the ND or the EMG envelope model-based (superscripts *ND* and *EMG*), while the subscript w indicates the whole contraction.

4. ${}^{ND}_{mw}R^2_g$ and ${}^{EMG}_{mw}R^2_g$ are the results of the global force estimation. The subscript g indicates the GLR model for the ND or the EMG model-based (superscripts *ND* and *EMG*), while the subscript mw indicates the moving window.

5. ${}^{ND_{GLR}}_{mw}R^2_{s/m/f}$ and ${}^{EMG_{GLR}}_{mw}R^2_{s/m/f}$ are the results of the estimations conducted by the global regressor on each individual force. The subscript GLR indicates the global model which estimates respectively the force of the contraction performed at fast (subscript f), medium (subscript m) and slow (subscript s). The subscript mw indicates the moving window.

A further statistical analysis was done considering separately the ND and the EMG envelope model-based. In this case, the statistical analysis was done comparing the ${}^{ND_{SLR}}_{mw}R^2_{s/m/f}$ with respect to ${}^{ND_{GLR}}_{mw}R^2_{s/m/f}$. The same statistical comparison for the EMG envelope model-based ${}^{EMG_{SLR}}_{mw}R^2_{s/m/f}$ with respect to ${}^{EMG_{GLR}}_{mw}R^2_{s/m/f}$. In this way it is assessed the statistical difference within the same model.

Chapter 7

Results and discussion

As presented in Chapter 6, the paired t-test was used to compare the statistical difference between the ND model-based and the EMG envelope model based. With the aim to help the reader and for a clearer discussion, the following nomenclature for the R^2 has been use in this chapter (also summarized in Fig. 7):

$$ {}^{ND/EMG_{SLR/GLR}}_{\quad w/mw}R^2_{s/m/f} \tag{7.1} $$

In particular, the design of the SLRs were done considering both the whole contraction (subscript w) and the moving window (subscript mw). Thus the first statistical comparison will be between ${}^{ND_{SLR}}_{w/mw}R^2_{s/m/f}$ and ${}^{EMG_{SLR}}_{w/mw}R^2_{s/m/f}$. A further statistical analysis will regard the GLRs, in particular the comparison between ${}^{ND}_{w/mw}R^2_g$ and ${}^{EMG}_{w/mw}R^2_g$.

In addition the last analysis will measure the performance of the global regressor in the IC estimations associated to slow, medium and fast speed of the contraction. Thus, the paired t-test was applied to assess the statistical differences between the ${}^{ND_{GLR}}_{mw}R^2_{s/m/f}$ and the ${}^{EMG_{GLR}}_{mw}R^2_{s/m/f}$.

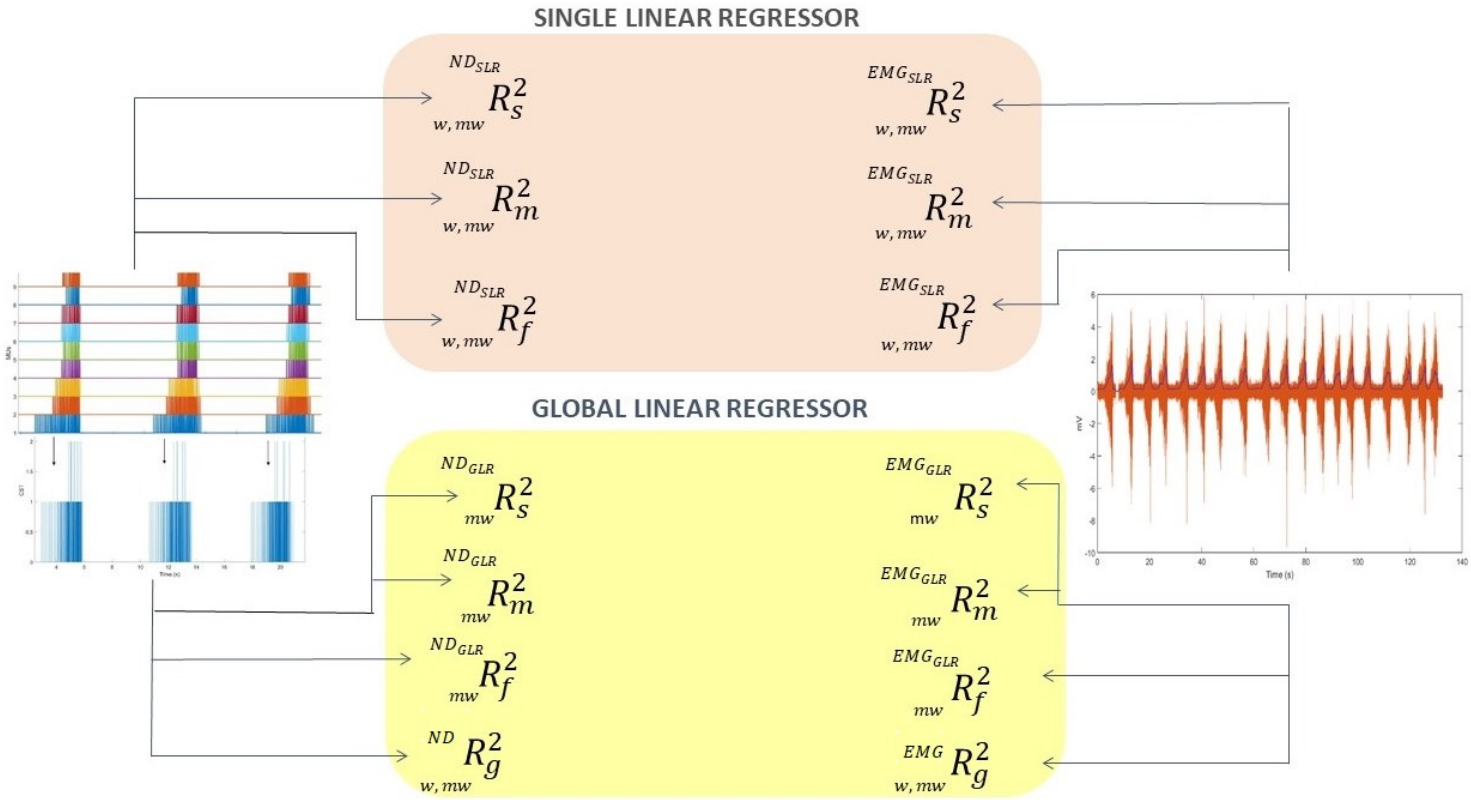

Figure 7.1. The block diagram summarize the R^2 values calculated to asses the performance of the designed regressor. Meaning of pedices and apices are the following: the left subscripts *mw* and *w* indicate respectively *whole* contraction and *moving window*; the right subscripts *s*, *m* and *f* indicate respectively *slow*, *medium* and *fast* speed of the contraction, The subscript on the left *GLR* and *SRL* indicate respectively the global and single linear regressor; finally the superscripts *ND* and *EMG* indicate respectively the neural drive and the EMG envelope to underlay the model used.

7.1 ${}^{ND_{SLR}}_{w}R^2_{s/m/f}$ versus ${}^{EMG_{SLR}}_{w}R^2_{s/m/f}$

The first analysis of the results considers the SLRs in order to show the effects that the different speeds have in the IC estimations (see Fig. 7.2 and 7.3). To quantify the performance of the regressions, the R^2 value was calculated. A strong positive association is found both for the ND and the EMG envelope model-based (see Tables 7.1). The mean R^2 values were always higher for the ND model-based (${}^{ND_{SLR}}_{w}R^2_s = 0{,}56$ vs ${}^{EMG_{SLR}}_{w}R^2_s = 0{,}47$; ${}^{ND_{SLR}}_{w}R^2_m = 0{,}50$ vs ${}^{EMG_{SLR}}_{w}R^2_m = 0{,}28$; ${}^{ND_{SLR}}_{w}R^2_f = 0{,}50$ vs ${}^{EMG_{SLR}}_{w}R^2_f = 0{,}53$). Indeed, the slope of the regressions obtained between IC and the EMG envelope model based (see Fig. 7.3) do not differ significantly from 0; that is particularly evident considering the medium and the fast speed of the contraction (see Fig. 7.3 red and blue regressions). This indicates the absence of a linear relationship (e.g. see in Table 7.1 the values of ${}^{EMG_{SLR}}_{w}R^2_m$ and ${}^{EMG_{SLR}}_{w}R^2_f$ reported for subject 1 and 2).

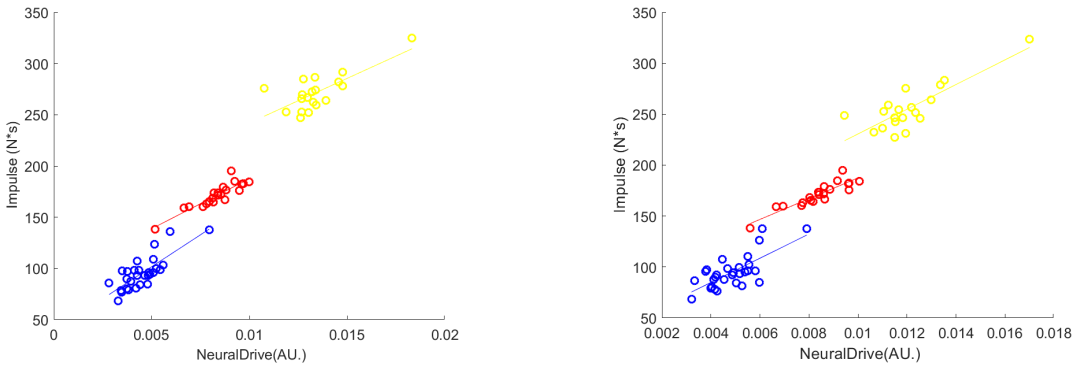

(a) (b)

Figure 7.2. Two examples of the regressions for the ND model-based. The regressions for the three speed of the contraction are depicted in different colours: slow speed in yellow, medium speed in red and fast speed in blue. The results shown are for two representative subjects.

To assess the statistical difference between the two models, the parametric paired t- test was used to statistically compared the R^2 values for each SLR among the 7 subjects. No statistical differences have been found between the EMG envelope model-based and the ND model-based ($p > 0.05$) (see Fig.7.4).

The relationships between IC and ND (see Fig. 7.2) show a clear discrimination between the levels of the speed and thus between the levels of force. This observation suggests that the three SLRs can be distributed along a single linear regressor, i.e. the GLR discussed in the next paragraph. Instead, from the relationships between IC and the EMG envelope these discriminations are not so evident. In particular, a complete overlap between the slow and the medium speed contraction is shown (in Fig. 7.3(b) represented by the regressions in yellow and in red). This

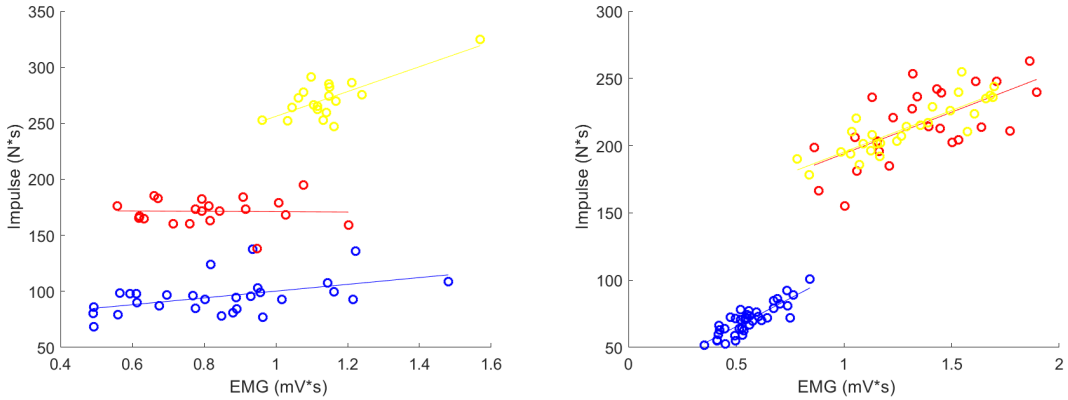

(a) (b)

Figure 7.3. Two examples of the regressions for the EMGe envelope model-based The regressions for the three speed of the contraction are depicted in different colours: slow speed in yellow, medium speed in red and fast speed in blue. The results shown are for two representative subjects.

Table 7.1. R^2 considering the entire ramp contraction for each single linear regression. Values per subject.

ND				EMG envelope			
Subj	${}^{ND_{SLR}}_{w}R^2_s$	${}^{ND_{SLR}}_{w}R^2_m$	${}^{ND_{SLR}}_{w}R^2_f$	Subj	${}^{EMG_{SLR}}_{w}R^2_s$	${}^{EMG_{SLR}}_{w}R^2_m$	${}^{EMG_{SLR}}_{w}R^2_f$
1	0,62	0,81	0,54	1	0,22	0	0,56
2	0,51	0,83	0,67	2	0,23	0	0,55
3	0,59	0,53	0,69	3	0,68	0,43	0,61
4	0,45	0,67	0,33	4	0,74	0,43	0,73
5	0,83	0,18	0,43	5	0,63	0,36	0,43
6	0,74	0,54	0,51	6	0,22	0,34	0,47
7	0,16	0,24	0,30	7	0,47	0,37	0,32
Mean	0,56	0,50	0,50	Mean	0,46	0,28	0,53

finding may be attributed to the amplitude cancellation that occurs when the positive and the negative phases of different MUAPs overlap and summate destructively (Boe *et al.*, 2008). Thus limits the possibility to understand the effects produced on the muscles activation considering the different speed of the contraction.

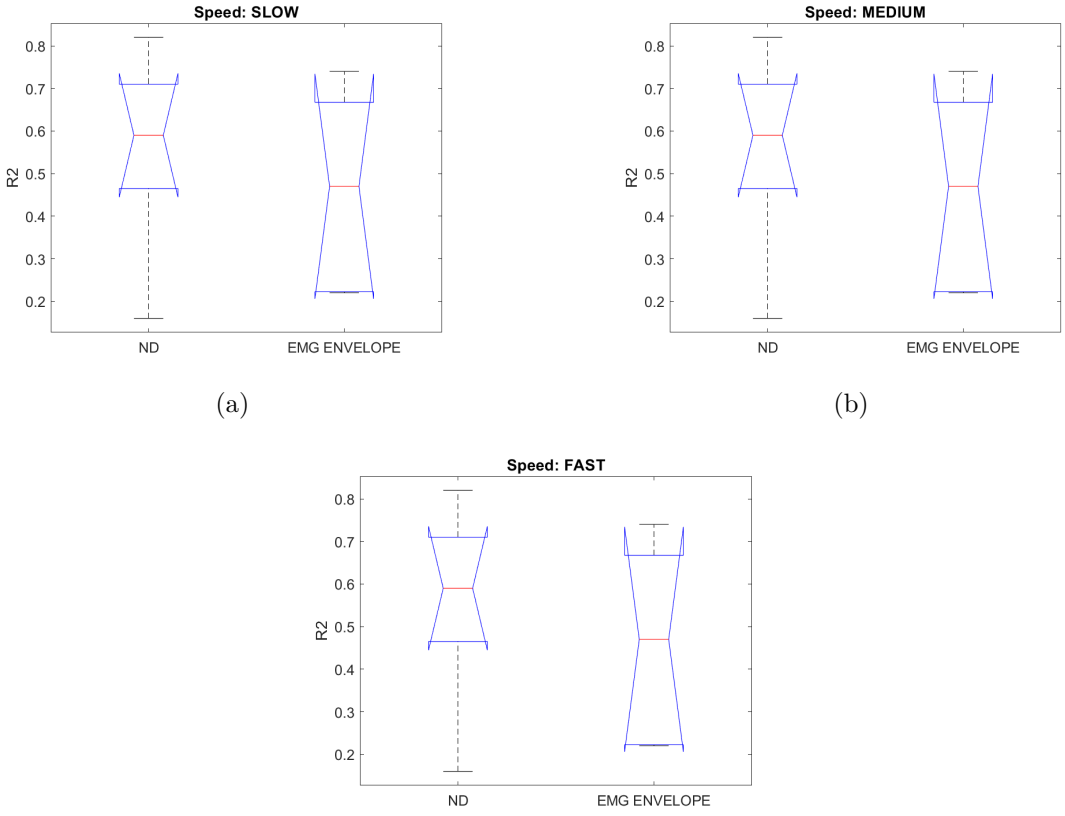

(a) (b)

(c)

Figure 7.4. Boxplots showing the ranges of R^2 obtained with the linear regressors.

7.2 ${}^{ND}_{w}R^2_g$ versus ${}^{EMG}_{w}R^2_g$

The design of the GLRs are due to the fact that in the event of implementing a controller able to control the force, the speed of the contraction is not known a priori. This means that, it is not possible to decide what type of regressor works better among the three available (see Fig. 7.5). A higher value of R^2 is obtained for the ND model-based ${}^{ND}_{w}R^2_g = 0{,}75$ and ${}^{EMG}_{w}R^2_g = 0{,}59$) although no statistical difference has been found (t test, p>0.05) (see Fig. 7.6).

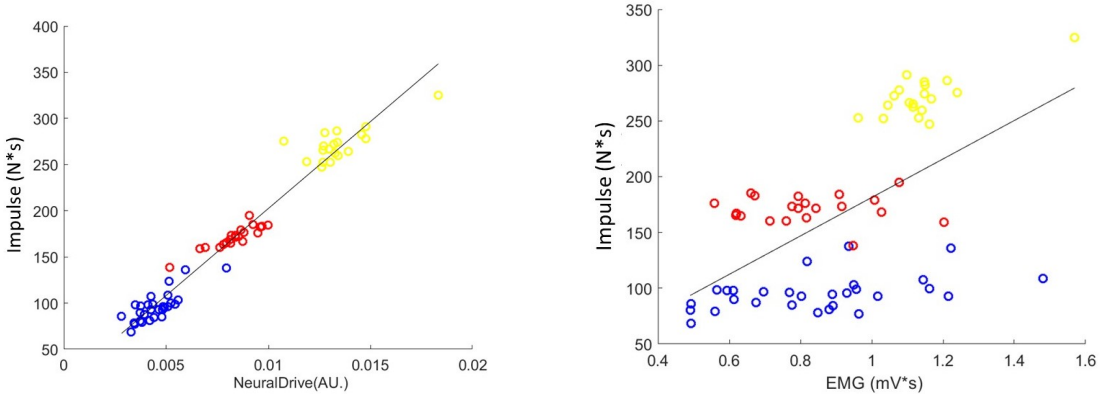

(a) (b)

Figure 7.5. In (a) total regressor based on 7.2 (a). In (b) total regressor based on 7.3 (a).

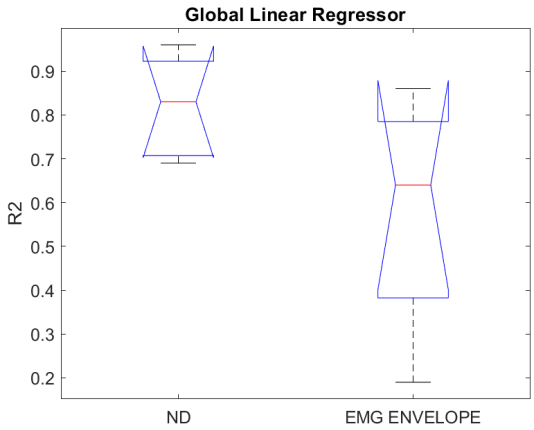

Figure 7.6. Boxplots showing the ranges of R^2 obtained with the global regressor

.

7.3 ${}^{ND_{SLR}}_{mw}R^2_{s/m/f}$ versus ${}^{EMG_{SLR}}_{mw}R^2_{s/m/f}$

Considering the case of using these force estimators for a myolectric control, the drawback due to the time delay (see Chapter 6) can be overcame considering a moving window of 200 ms. Thus, three SLRs are designed for the ND and the EMG envelope model-based (see Fig. 7.7).

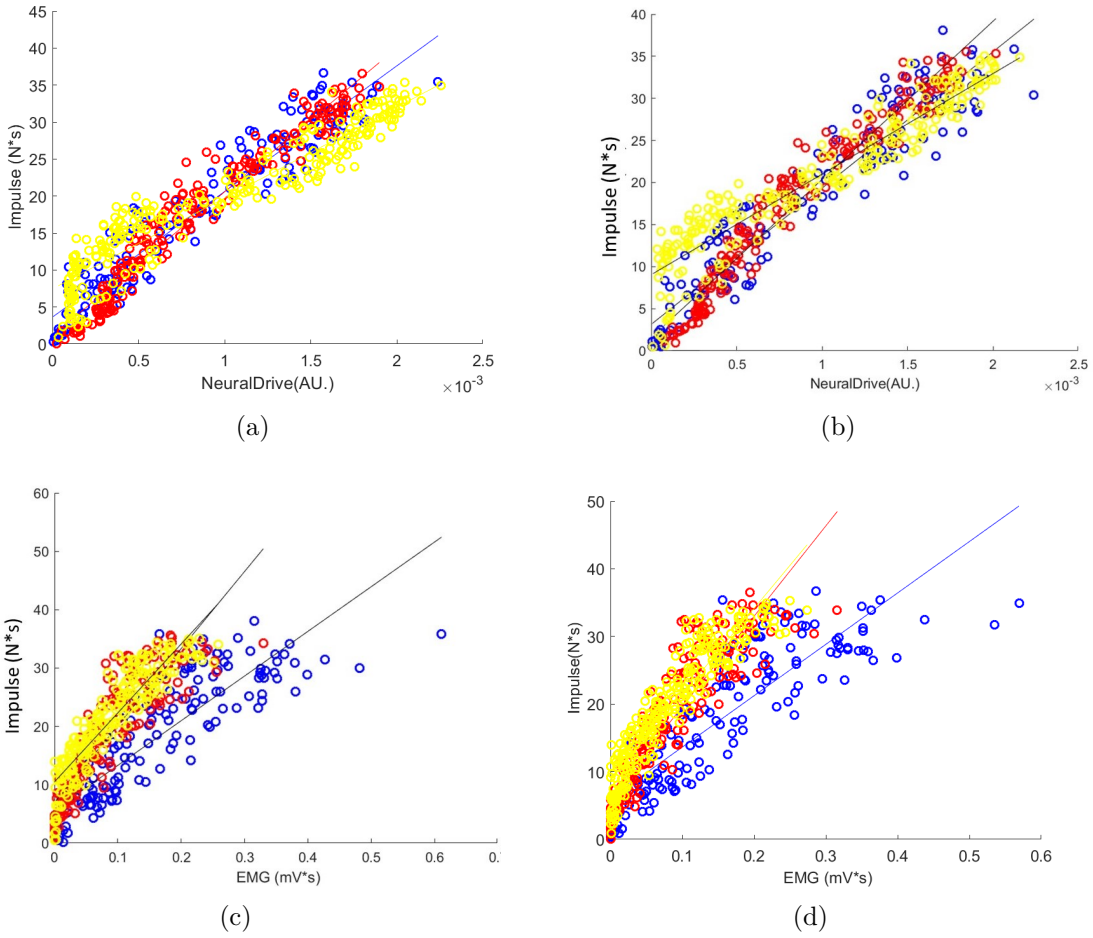

Figure 7.7. Four examples of the regressions used to estimate the contractile impulse. In (a) and (b) the ND model-based; in (c) and (d) the EMG envelope model-based. The regressions for the three speed of the contraction are depicted in different colours: slow speed in yellow, medium speed in red and fast speed in blue. The results shown are for two representative subjects.

The mean R^2 values were always higher for the ND model-based (${}^{ND_{SLR}}_{mw}R^2_s$ = 0,88 vs ${}^{EMG_{SLR}}_{mw}R^2_s$ = 0,80; ${}^{ND_{SLR}}_{mw}R^2_m$ = 0,87 vs ${}^{EMG_{SLR}}_{mw}R^2_m$ = 0,77; ${}^{ND_{SLR}}_{mw}R^2_f$= 0,87 vs ${}^{EMG_{SLR}}_{mw}R^2_f$ = 0,79). In this case, these observations show a significant statistical difference ($p < 0.05$) obtained comparing the two models in th three different conditions (i.e. slow, fast, medium and global) (see Fig. 7.8).

Table 7.2. R^2 considering 200ms window. Values per subject.

ND				EMG envelope			
Subj	${}^{ND_{SLR}}_{mw}R^2_s$	${}^{ND_{SLR}}_{mw}R^2_m$	${}^{ND_{SLR}}_{mw}R^2_f$	Subj	${}^{EMG_{SLR}}_{mw}R^2_s$	${}^{EMG_{SLR}}_{mw}R^2_m$	${}^{EMG_{SLR}}_{mw}R^2_f$
1	0,91	0,95	0,90	1	0,74	0,81	0,85
2	0,90	0,95	0,90	2	0,75	0,80	0,82
3	0,87	0,82	0,85	3	0,84	0,75	0,78
4	0,93	0,91	0,92	4	0,87	0,73	0,74
5	0,93	0,87	0,86	5	0,83	0,80	0,79
6	0,81	0,86	0,82	6	0,71	0,73	0,72
7	0,78	0,72	0,84	7	0,85	0,74	0,79
Mean	0,88	0,87	0,87	Mean	0,80	0,77	0,79

In this way, the higher R^2 mean value obtained with the ND model-based assumes statistical significance. Indeed, the ND model-based is more sensitive to the small changes in the IC considering the low speed of the contraction (see Fig. 7.7(a) and (b) regressions in the yellow) with respect to the EMG envelope model based. Indeed, the increasing in IC $\sim$ 5-15 Ns are not follow by a correspondent increase in EMG envelope ($\sim$ 0 mVs) (see Fig. 7.7(c) and (d) regressions in yellow and red represent respectively the contractions performed at slow and medium speed (20%MVC/s, 30%MVC/s)). These results can be explained considering the low-threshold motor units recruited for slow levels of the force. These MUs produce smaller surface action potentials with respect to the high threshold MUs; thus their effect is more reduced by the amplitude cancellation.

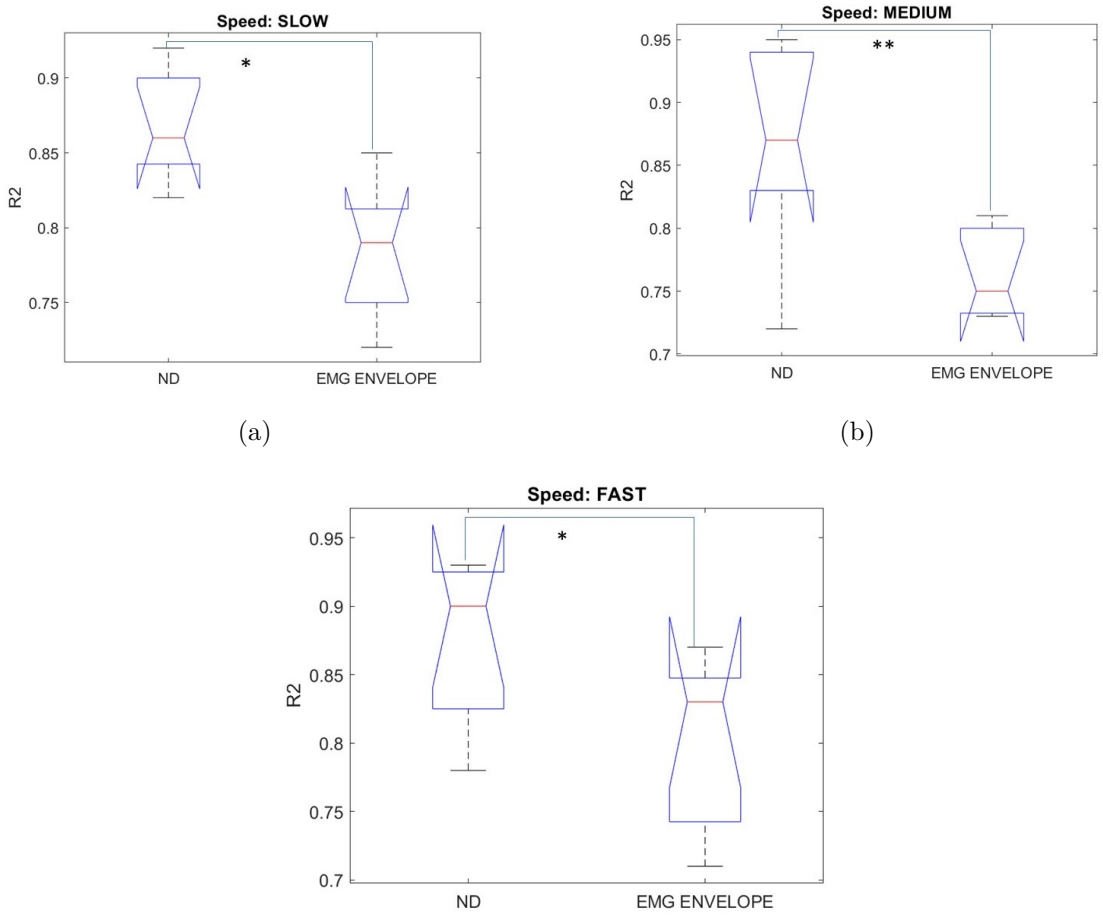

(a) (b)

(c)

Figure 7.8. Boxplots showing the ranges of R^2 obtained with the single linear regressors. According to the convention symbol used in statistic, * indicates a p value < 0.05 while ** indicates a p value < 0.01.

7.4 ${}^{ND}_{w}R^2_g$ versus ${}^{EMG}_{w}R^2_g$

The GLRs (see Fig. 7.9) performance were measured in term of R^2. A higher value of R^2 is obtained from the ND model-based (${}^{ND}_{mw}R^2$= 0,81 and ${}^{EMG}_{mw}R^2$ = 0,69) and a significant statistical differences ($p < 0.05$) is founded between the two models (see Fig. 7.10).

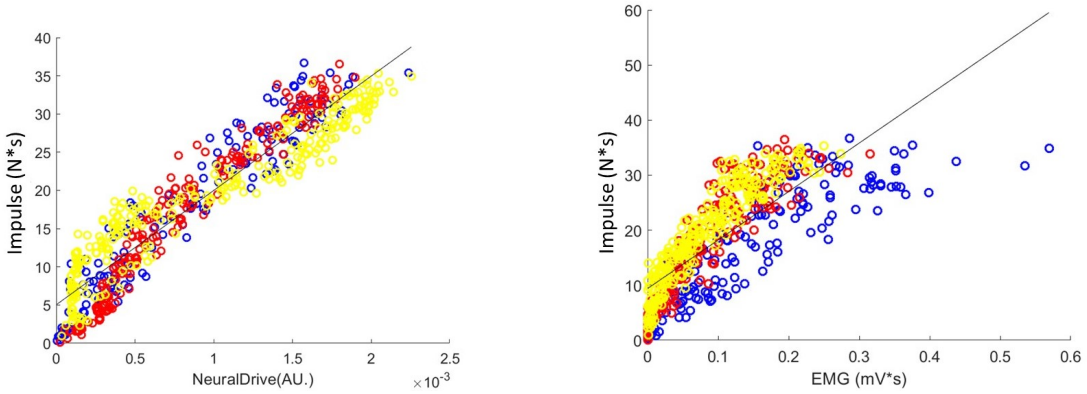

(a) (b)

Figure 7.9. In (a) the global regressor obtained with the ND model-based; in (b) the global regressor obtained with the EMG envelope model-based.

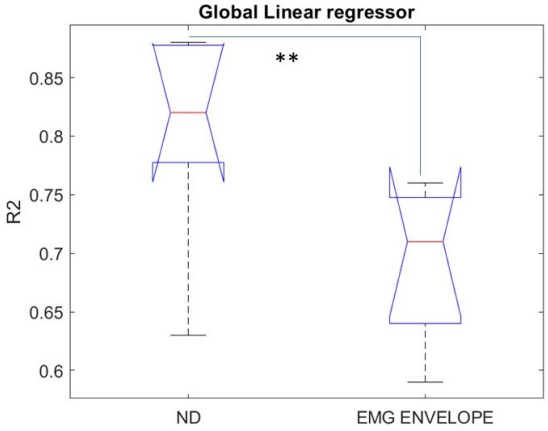

Figure 7.10. Boxplot shows the ranges of R^2 obtained with the global regressor. According to the convention symbol used in statistic, ** indicates a p value < 0.01.

7.5 Statistical analysis: ${}^{ND_{GLR}}_{mw}R^2_{s/m/f}$ versus ${}^{EMG_{GLR}}_{mw}R^2_{s/m/f}$

In the last analysis the ${}^{ND_{GLR}}_{mw}R^2_{s/m/f}$ and ${}^{EMG_{GLR}}_{mw}R^2_{s/m/f}$ were calculated. This means to measure how each independent variable (IC slow, IC medium, IC fast) is estimated by the global estimator. Thus, the paired t-test was applied to assess the statistical differences between the two model. A positive association, in terms of R^2, is found both for the ND and the EMG envelope model-based (see Tables 7.3). Higher R^2 mean values are obtained from the ND model-based (${}^{ND_{GLR}}_{mw}R^2_s = 0{,}77$ vs ${}^{EMG_{GLR}}_{mw}R^2_s = 0{,}6$; ${}^{ND_{GLR}}_{mw}R^2_m = 0{,}82$ vs ${}^{EMG_{GLR}}_{mw}R^2_m = 0.72$; ${}^{ND_{GLR}}_{mw}R^2_f = 0.77$ vs ${}^{EMG_{GLR}}_{mw}R^2_{s,m,f} = 0.68$). In particular, a significant statistical difference is observed by comparing the ${}^{ND_{GLR}}_{mw}R^2_s$ versus ${}^{EMG_{GLR}}_{mw}R^2_s$ and ${}^{ND_{GLR}}_{mw}R^2_m$ versus ${}^{EMG_{GLR}}_{mw}R^2_m$; while there is no significant statistical difference between ${}^{ND_{GLR}}_{mw}R^2_f$ and ${}^{EMG_{GLR}}_{mw}R^2_f$ (see Tables 7.11).

Table 7.3. R^2 considering the estimation of the global model for each different speed. Values per subject.

ND				EMG			
Subj	${}^{ND_{GLR}}_{mw}R^2_s$	${}^{ND_{GLR}}_{mw}R^2_m$	${}^{ND_{GLR}}_{mw}R^2_f$	Subj	${}^{EMG_{GLR}}_{mw}R^2_s$	${}^{EMG_{GLR}}_{mw}R^2_m$	${}^{EMG_{GLR}}_{mw}R^2_f$
1	0,89	0,90	0,86	1	0,46	0,71	0,69
2	0,89	0,91	0,82	2	0,46	0,68	0,59
3	0,79	0,81	0,82	3	0,65	0,73	0,69
4	0,90	0,76	0,63	4	0,67	0,73	0,63
5	0,87	0,85	0,87	5	0,70	0,74	0,78
6	0,32	0,79	0,59	6	0,48	0,70	0,62
7	0,74	0,71	0,83	7	0,75	0,74	0,77
Mean	0,77	0,82	0,77	Mean	0,60	0,72	0,68

Finally, a paired t-test was applied to assess the differences in performance inside the same model. This means to compare the estimation of the force, at a certain speed of the contraction, both using the single SLR and the GLR (see Tables 7.4 and 7.5). A higher R^2 mean values is reported for the SLRs based on the EMG envelope (${}^{EMG_{SLR}}_{mw}R^2_s = 0{,}80$ vs ${}^{EMG_{GLR}}_{mw}R^2_s = 0{,}6$; ${}^{EMG_{SLR}}_{mw}R^2_m = 0{,}77$ vs ${}^{EMG_{GLR}}_{mw}R^2_m = 0.72$; ${}^{EMG_{SLR}}_{mw}R^2_f = 0{,}79$ vs ${}^{EMG_{GLR}}_{mw}R^2_f = 0.68$) and a significant statistical differences is obtained comparing the different R^2 mean values (see Fig. 7.12). On the contrary, considering the ND model-based no significant statistical difference in shown (see Fig. 7.13).

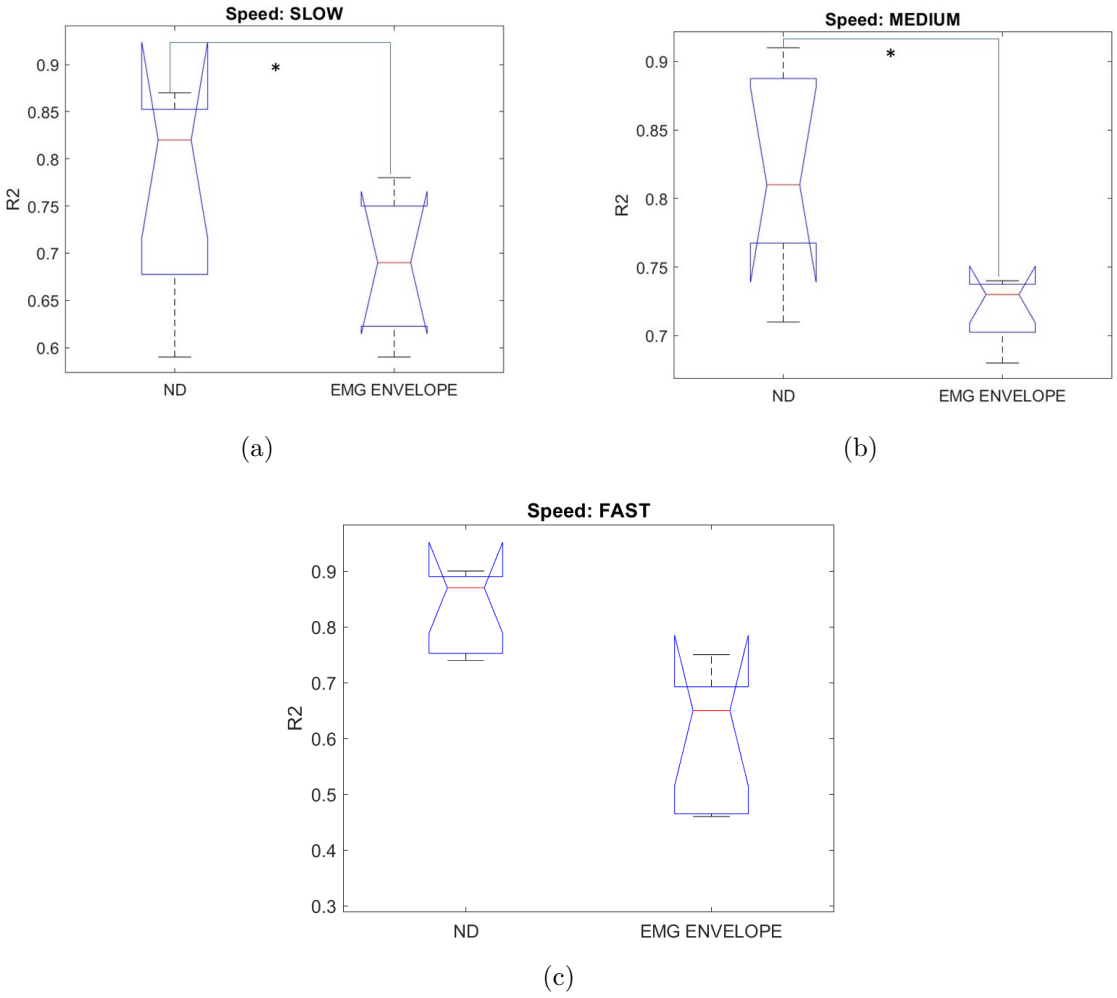

Figure 7.11. Boxplots showing the ranges of R^2 obtained with the global regressor In (c) there is no significance statistical difference.

Table 7.4. R^2 considering 200ms window. Values per subject. Table on the left indicates the R^2 for the each SLRs, while the table on the right indicates the R^2 obtained estimating each single force by the GLR.

ND			
Subj	${}^{ND_{SLR}}_{mw}R^2_s$	${}^{ND_{SLR}}_{mw}R^2_m$	${}^{ND_{SLR}}_{mw}R^2_f$
1	0,91	0,95	0,90
2	0,90	0,95	0,90
3	0,87	0,82	0,85
4	0,93	0,91	0,92
5	0,93	0,87	0,86
6	0,81	0,86	0,82
7	0,78	0,72	0,84
Mean	0,88	0,87	0,87

ND			
Subj	${}^{ND_{GLR}}_{mw}R^2_s$	${}^{ND_{GLR}}_{mw}R^2_m$	${}^{ND_{GLR}}_{mw}R^2_f$
1	0,89	0,90	0,86
2	0,89	0,91	0,82
3	0,79	0,81	0,82
4	0,90	0,76	0,63
5	0,87	0,85	0,87
6	0,32	0,79	0,59
7	0,74	0,71	0,83
Mean	0,77	0,82	0,77

Table 7.5. R^2 considering 200ms window. Values per subject. Table on the left indicates the R^2 for the each SLRs, while the table on the right indicates the R^2 obtained estimating each single force by the GLR.

EMG envelope			
Subj	${}^{EMG_{SLR}}_{mw}R^2_s$	${}^{EMG_{SLR}}_{mw}R^2_m$	${}^{EMG_{SLR}}_{mw}R^2_f$
1	0,74	0,81	0,85
2	0,75	0,80	0,82
3	0,84	0,75	0,78
4	0,87	0,73	0,74
5	0,83	0,80	0,79
6	0,71	0,73	0,72
7	0,85	0,74	0,79
Mean	0,80	0,77	0,79

EMG envelope			
Subj	${}^{EMG_{GLR}}_{mw}R^2_s$	${}^{EMG_{GLR}}_{mw}R^2_m$	${}^{EMG_{GLR}}_{mw}R^2_f$
1	0,46	0,71	0,69
2	0,46	0,68	0,59
3	0,65	0,73	0,69
4	0,67	0,73	0,63
5	0,70	0,74	0,78
6	0,48	0,70	0,62
7	0,75	0,74	0,77
Mean	0,60	0,72	0,68

This is an important results, since we can use the ND global linear regressor to estimate different levels of force at different speed, with a fair trade-off among the three conditions. In fact, with the EMG SLR model based, we had better performance in each condition with respect to the EMG global linear regressor. While, considering the ND global linear regressor, no statistical difference is shown. This, making the ND global linear regressor more suitable in unknown velocity condition.

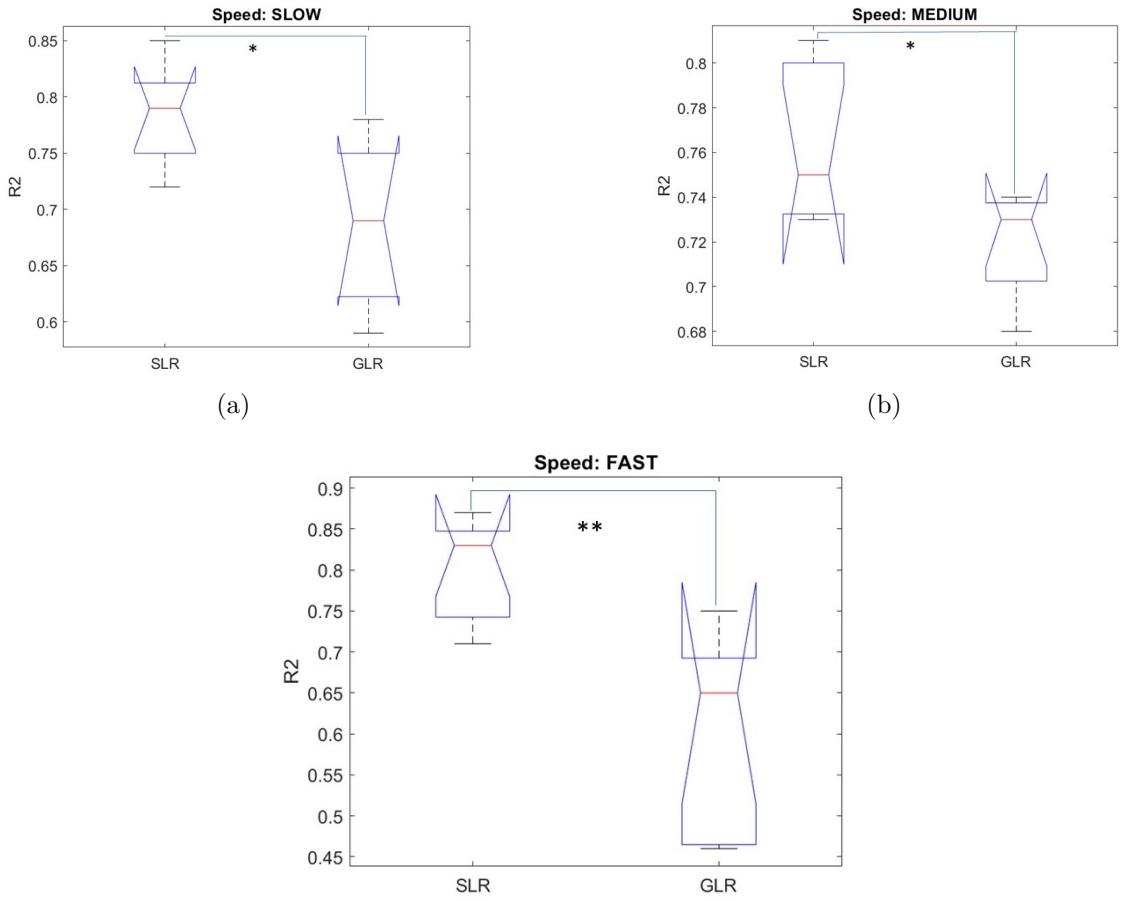

Figure 7.12. Boxplots showing the ranges of R^2 obtained with the global regressor and the single linear regressions using the EMG model-based.

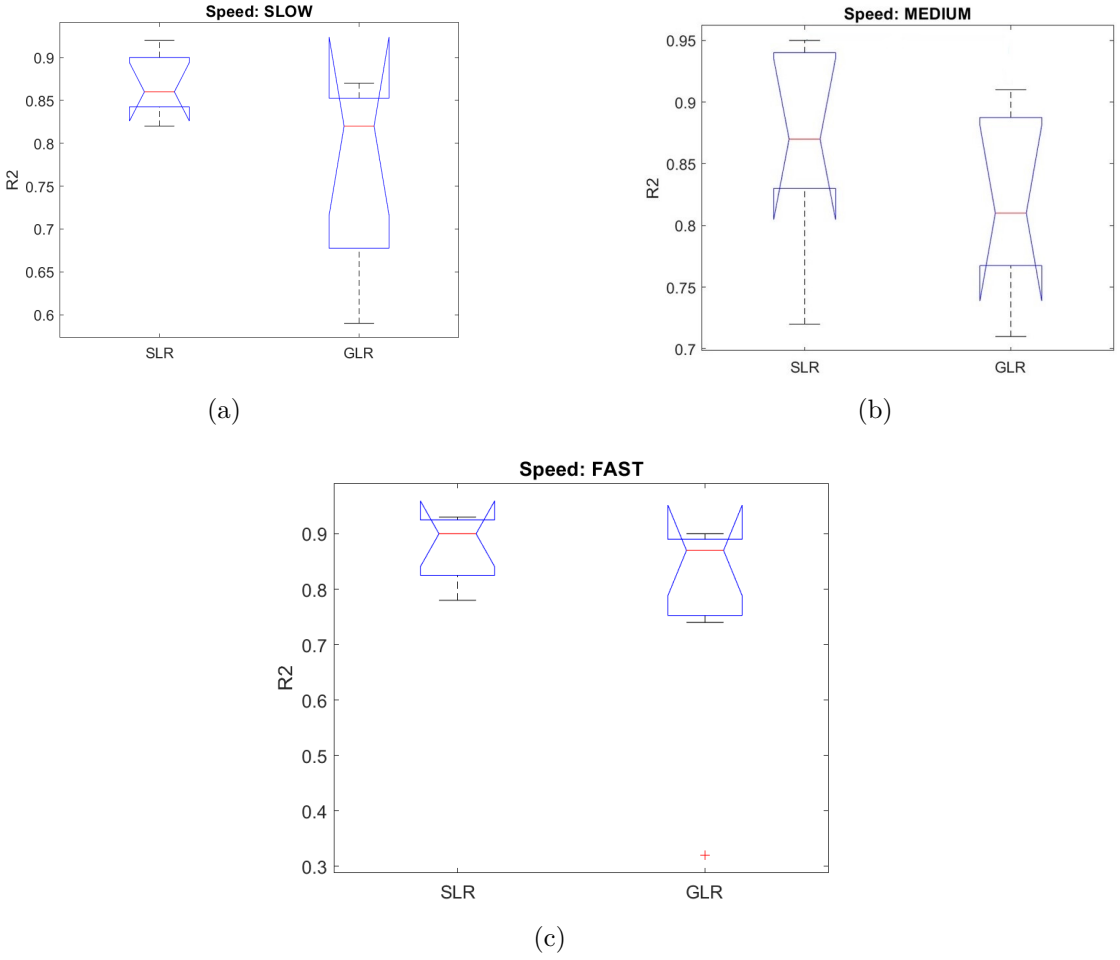

(a) (b) (c)

Figure 7.13. Boxplots showing the ranges of R^2 obtained with the global regressor and the single linear regressions using the ND model-based.

Chapter 8

Conclusion and future developments

The investigations undertaken in this project range from the research in motor neuroscience to the possible technology applications in the field of motor rehabilitation. In particular, the understanding of the motor unit behaviour, thanks to the surface EMG decomposition, allows both to explore the motor neurons activity and to extract the neural drive to muscles. Indeed, in the perspective of advancing technologies based on the neural feature as the smoothed cumulative spike timings a knowledge of the neuromechanical principles underlying the neural functions is needed. In this view, the development of a human-machine interfaces for robotic limbs and exoskeletons is possible. For this purpose, the offline high-density EMG signals decomposition is used in this work to understand the basis of the neurophysiology of movement. The feasibility to estimate the muscle force in terms of contractile impulse using the neural drive model-base is demonstrated by the higher R^2 values with respect to the EMG envelope model-based. The two different force estimators are compared considering single linear regression (based on different velocities) and the global linear regressor, evaluating the performance along all the time contraction and in a time window of 200 ms. The choose to estimate the single forces allowed to test the addresses of the motor units in specific condition and thus the capability to predict the force output. At the same time, considering the event of a prosthetic implementation, the huma-machine interface should overcome challenges as the time delay or the possibility to estimate different level of force with a global estimator producing low estimation errors. The outcomes show how using a time window of 200 ms the ND model-based estimator provides accurate information for different levels of contraction speed, in particular the reliability is obtained considering the small increases of force. This is an important achievement which can be reached by using the EMG envelope. In fact, by using the last, the contribution of the low threshold motor unit may be lost because of the very low intensity of the action potential. In this way, the estimation of low level forces

may be incorrect. On the contrary the MUs spike activity provide the drive signals that can replicate the limb movement in a proportional way. The proportionality is given by the high sensibility to different force levels and in the the possibility to associated the neural occurrences to a specific task. This last observation includes to test the the force estimation in different degree of freedom (DoF) (Kapelner *et al.*, 2018).

Unfortunately, constraints on time and facilities limited both the number and the different ankle dorsi-flexion joint angular positions that could be tested in this work. Indeed, starting from this results it may be possible to test the decomposition including the motion capture system at different ankle joint arrangements and with regression methods to estimate the joint kinematics. Finally, the presented results are limited to an offline analysis and to the stationary conditions (isometric contraction). A further developments could explore the on line decomposition and dynamic contraction.

Bibliography

Binder, Marc, Heckman, Cj, & Powers, Randall. 1996. The physiological control of motoneuron activity. Handbook of Physiology. Exercise: Regulation and Integration of Maltiple Systems. *Bethesda: Am. Physiol. Soc*, 01, 3–53.

Boe, S. G., Rice, C. L., & Doherty, T. J. 2008. Estimating contraction level using root mean square amplitude in control subjects and patients with neuromuscular disorders. *Arch Phys Med Rehabil*, **89**(4), 711–718.

Burke, R. E., Strick, P. L., Kanda, K., Kim, C. C., & Walmsley, B. 1977. Anatomy of medial gastrocnemius and soleus motor nuclei in cat spinal cord. *J. Neurophysiol.*, **40**(3), 667–680.

Day, Scott, & Hulliger, Manuel. 2001. Experimental Simulation of Cat Electromyogram: Evidence for Algebraic Summation of Motor-Unit Action-Potential Trains. *Journal of neurophysiology*, **86**(12), 2144–58.

De Luca, C. J., & Contessa, P. 2012. Hierarchical control of motor units in voluntary contractions. *J. Neurophysiol.*, **107**(1), 178–195.

De Luca, C. J., & Erim, Z. 1994. Common drive of motor units in regulation of muscle force. *Trends Neurosci.*, **17**(7), 299–305.

De Luca, C. J., & Hostage, E. C. 2010. Relationship between firing rate and recruitment threshold of motoneurons in voluntary isometric contractions. *J. Neurophysiol.*, **104**(2), 1034–1046.

De Luca, C. J., & Merletti, R. 1988. Surface myoelectric signal cross-talk among muscles of the leg. *Electroencephalogr Clin Neurophysiol*, **69**(6), 568–575.

De Luca, C. J., Gilmore, L. D., Kuznetsov, M., & Roy, S. H. 2010. Filtering the surface EMG signal: Movement artifact and baseline noise contamination. *J Biomech*, **43**(8), 1573–1579.

Del Vecchio, A., Casolo, A., Negro, F., Scorcelletti, M., Bazzucchi, I., Enoka, R., Felici, F., & Farina, D. 2019a. The increase in muscle force after 4 weeks of

strength training is mediated by adaptations in motor unit recruitment and rate coding. *J. Physiol. (Lond.)*, **597**(7), 1873–1887.

Del Vecchio, Alessandro, Úbeda, Andrés, Sartori, Massimo, Azorin, Jose, Felici, Francesco, & Farina, Dario. 2018. The Central Nervous System Modulates the Neuromechanical Delay in a Broad Range for the Control of Muscle Force. *Journal of Applied Physiology*, **125**(07).

Del Vecchio, Alessandro, Negro, Francesco, Holobar, Ales, Casolo, Andrea, P Folland, Jonathan, Felici, Francesco, & Farina, Dario. 2019b. You are as fast as your motor neurons: Speed of recruitment and maximal discharge of motor neurons determine the maximal rate of force development in humans. *The Journal of Physiology*, 02.

Dimitrova, N.A., & Dimitrov, G.V. 2002. Amplitude-related characteristics of motor unit and M-wave potentials during fatigue. A simulation study using literature data on intracellular potential changes found in vitro. *Journal of Electromyography and Kinesiology*, **12**(5), 339 – 349.

Drost, G., Stegeman, D. F., van Engelen, B. G., & Zwarts, M. J. 2006. Clinical applications of high-density surface EMG: a systematic review. *J Electromyogr Kinesiol*, **16**(6), 586–602.

Duchateau, J., & Enoka, R. M. 2011. Human motor unit recordings: origins and insight into the integrated motor system. *Brain Res.*, **1409**(Aug), 42–61.

Farina, D., & Enoka, R. M. 2011. Surface EMG decomposition requires an appropriate validation. *J. Neurophysiol.*, **105**(2), 981–982.

Farina, D., Negro, F., Gazzoni, M., & Enoka, R. M. 2008. Detecting the unique representation of motor-unit action potentials in the surface electromyogram. *J. Neurophysiol.*, **100**(3), 1223–1233.

Farina, D., Holobar, A., Merletti, R., & Enoka, R. M. 2010. Decoding the neural drive to muscles from the surface electromyogram. *Clin Neurophysiol*, **121**(10), 1616–1623.

Farina, D., Negro, F., & Dideriksen, J. L. 2014. The effective neural drive to muscles is the common synaptic input to motor neurons. *J. Physiol. (Lond.)*, **592**(16), 3427–3441.

Farina, Dario, Vujaklija, Ivan, Sartori, Massimo, Kapelner, Tamás, Negro, Francesco, Jiang, Ning, Bergmeister, Konstantin, Andalib, Arash, Principe, Jose, & Aszmann, Oskar C. 2017. Man/machine interface based on the discharge timings of spinal motor neurons after targeted muscle reinnervation. *Nature Biomedical Engineering*, **1**.

Farrell, Todd R., & Weir, Richard F. 2008. ANALYSIS WINDOW INDUCED CONTROLLER DELAY FOR MULTIFUNCTIONAL PROSTHESES.

Fyffe, R.E.W. 2001. *Spinal motoneurons: Synaptic inputs and receptor organization.* Pages 21–46.

H. Blok, J, van dijk, Johannes, Drost, Gea, J. Zwarts, M, & Stegeman, Dick. 2002. A high-density multichannel surface electromyography system for the characterization of single motor units. *Review of Scientific Instruments*, **73**(04), 1887–1897.

Hakonen, Maria, Piitulainen, Harri, & Visala, Arto. 2015. Current state of digital signal processing in myoelectric interfaces and related applications. *Biomedical Signal Processing and Control*, **18**, 334 – 359.

Heckman, C.J., & Enoka, Roger. 2012. Motor Unit. *Comprehensive Physiology*, **2**(10), 2629–2682.

Heckman, C.J., & Enoka, Roger M. 2004. Physiology of the motor neuron and the motor unit. *Pages 119 – 147 of:* Eisen, Andrew (ed), *Clinical Neurophysiology of Motor Neuron Diseases.* Handbook of Clinical Neurophysiology, vol. 4. Elsevier.

Hodges, P. W., & Bui, B. H. 1996. A comparison of computer-based methods for the determination of onset of muscle contraction using electromyography. *Electroencephalogr Clin Neurophysiol*, **101**(6), 511–519.

Hogrel, J. Y. 2005. Clinical applications of surface electromyography in neuromuscular disorders. *Neurophysiol Clin*, **35**(2-3), 59–71.

Holobar, A., & Farina, D. 2014. Blind source identification from the multichannel surface electromyogram. *Physiol Meas*, **35**(7), R143–165.

Holobar, A., & Zazula, D. 2007. Multichannel Blind Source Separation Using Convolution Kernel Compensation. *IEEE Transactions on Signal Processing*, **55**(9), 4487–4496.

Holobar, A., Minetto, M. A., & Farina, D. 2014. Accurate identification of motor unit discharge patterns from high-density surface EMG and validation with a novel signal-based performance metric. *J Neural Eng*, **11**(1), 016008.

Holobar, Ales, & Zazula, Damjan. 2007 (09). Gradient Convolution Kernel Compensation Applied to Surface Electromyograms.

Hu, Xiaogang, Rymer, William Z., & Suresh, Nina L. 2014. Control of motor unit firing during step-like increases in voluntary force. *Frontiers in Human Neuroscience*, **8**, 721.

Kallenberg, L. A., & Hermens, H. J. 2006. Behaviour of motor unit action potential rate, estimated from surface EMG, as a measure of muscle activation level. *J Neuroeng Rehabil*, **3**(Jul), 15.

Kapelner, T., Negro, F., Aszmann, O. C., & Farina, D. 2018. Decoding Motor Unit Activity From Forearm Muscles: Perspectives for Myoelectric Control. *IEEE Trans Neural Syst Rehabil Eng*, **26**(1), 244–251.

Kapelner, T., Vujaklija, I., Jiang, N., Negro, F., Aszmann, O. C., Principe, J., & Farina, D. 2019. Predicting wrist kinematics from motor unit discharge timings for the control of active prostheses. *J Neuroeng Rehabil*, **16**(1), 47.

Keenan, K. G., Farina, D., Merletti, R., & Enoka, R. M. 2006. Amplitude cancellation reduces the size of motor unit potentials averaged from the surface EMG. *J. Appl. Physiol.*, **100**(6), 1928–1937.

Kernell, D. 1992. Organized variability in the neuromuscular system: a survey of task-related adaptations. *Arch Ital Biol*, **130**(1), 19–66.

Lefever, R. S., & De Luca, C. J. 1982. A Procedure for Decomposing the Myoelectric Signal Into Its Constituent Action Potentials - Part I: Technique, Theory, and Implementation. *IEEE Transactions on Biomedical Engineering*, **BME-29**(3), 149–157.

Mambrito, B., & De Luca, C. J. 1984. A technique for the detection, decomposition and analysis of the EMG signal. *Electroencephalogr Clin Neurophysiol*, **58**(2), 175–188.

Martinez-Valdes, E., Negro, F., Laine, C. M., Falla, D., Mayer, F., & Farina, D. 2017. Tracking motor units longitudinally across experimental sessions with high-density surface electromyography. *J. Physiol. (Lond.)*, **595**(5), 1479–1496.

Masakado, Y., Akaboshi, K., Nagata, M., Kimura, A., & Chino, N. 1995. Motor unit firing behavior in slow and fast contractions of the first dorsal interosseous muscle of healthy men. *Electroencephalogr Clin Neurophysiol*, **97**(6), 290–295.

Merletti, R., & Farina, D. 2009. Analysis of intramuscular electromyogram signals. *Philos Trans A Math Phys Eng Sci*, **367**(1887), 357–368.

Merletti, R., Holobar, A., & Farina, D. 2008. Analysis of motor units with high-density surface electromyography. *J Electromyogr Kinesiol*, **18**(6), 879–890.

Muceli, Silvia, Poppendieck, Wigand, Negro, Francesco, Yoshida, Ken, Hoffmann, Klaus-Peter, Butler, Jane, Gandevia, Simon, & Farina, Dario. 2015. Accurate and representative decoding of the neural drive to muscles in humans with multi-channel intramuscular thin-film electrodes. *The Journal of physiology*, **593**(07).

Naik, G. R., Selvan, S. E., Gobbo, M., Acharyya, A., & Nguyen, H. T. 2016. Principal Component Analysis Applied to Surface Electromyography: A Comprehensive Review. *IEEE Access*, **4**, 4025–4037.

Negro, F., Muceli, S., Castronovo, A. M., Holobar, A., & Farina, D. 2016. Multi-channel intramuscular and surface EMG decomposition by convolutive blind source separation. *J Neural Eng*, **13**(2), 026027.

Sartori, M., Yavuz, U., & Farina, D. 2017. In Vivo Neuromechanics: Decoding Causal Motor Neuron Behavior with Resulting Musculoskeletal Function. *Sci Rep*, **7**(1), 13465.

Staudenmann, D., Kingma, I., Daffertshofer, A., Stegeman, D. F., & van Dieen, J. H. 2006. Improving EMG-based muscle force estimation by using a high-density EMG grid and principal component analysis. *IEEE Trans Biomed Eng*, **53**(4), 712–719.

Stoykov, N. S., Lowery, M. M., Heckman, C. J., Taflove, A., & Kuiken, T. A. 2005 (June). Recording intramuscular EMG signals using surface electrodes. *Pages 291–294 of: 9th International Conference on Rehabilitation Robotics, 2005. ICORR 2005.*

Tedroff, K., Knutson, L. M., & Soderberg, G. L. 2006. Synergistic muscle activation during maximum voluntary contractions in children with and without spastic cerebral palsy. *Dev Med Child Neurol*, **48**(10), 789–796.

Twardowski, M. D., Roy, S. H., Li, Z., Contessa, P., De Luca, G., & Kline, J. C. 2019. Motor unit drive: a neural interface for real-time upper limb prosthetic control. *J Neural Eng*, **16**(1), 016012.

Van Cutsem, M., & Duchateau, J. 2005. Preceding muscle activity influences motor unit discharge and rate of torque development during ballistic contractions in humans. *J. Physiol. (Lond.)*, **562**(Pt 2), 635–644.

Van Cutsem, M., Duchateau, J., & Hainaut, K. 1998. Changes in single motor unit behaviour contribute to the increase in contraction speed after dynamic training in humans. *J. Physiol. (Lond.)*, **513 (Pt 1)**(Nov), 295–305.

Acknowledgements

Ci siamo. Con la musica nelle orecchie voglio riavvolgere il nastro di questi mesi e di questi anni.

Ringrazio il mio professore e relatore Marco Gazzoni. Grazie perché con lei e con le sue lezioni ho capito cosa amo del mio percorso di studi. Sono certa che in questi mesi ogni suo sorriso voleva rassicurare le mie paure e le mie insicurezze. Grazie per la pazienza, la calma e la gentilezza che la contraddistinguono. Ringrazio tutti i ragazzi e i dottorandi del Lisin, siete un gruppo fantastico.

Ringrazio il mio secondo relatore, il professore Dario Farina è stato un onore poter lavorare con voi. Un grazie particolare va ai miei tutor Silvia ed Alessandro, che più da vicino mi hanno seguita in questo lavoro.

Il ringraziamento più grande va alla mia famiglia, a voi devo tutto. Grazie ai miei genitori per aver creduto sempre in me, per aver avuto sempre una gamba più lunga della mia, per aver affrontato con me ogni sessione d'esame, ogni sconfitta e ogni vittoria. Grazie mamma per essere il mio esempio di forza e grazie papà per i baci della buonanotte che sono la costante silenziosa di ogni sera che la freccia bianca mi riporta a casa. Grazie a mia sorella Joanna. Senza di lei tante situazioni non avrei saputo affrontarle. Grazie per avermi sempre appoggiata nelle mie scelte, giuste e sbagliate, per i tuoi "Marià te l'avevo detto!", per avermi insegnato a contare fino a dieci. Grazie per essere la mia piccola grande donna. Grazie a zia Anna e zio Tonino che tra i loro duemila impegni sono riusciti a farmi felice. Siete la mia seconda casa.

Ringrazio la mia super cugina-sorella acquisita Daria. Grazie per le lunghe chicchierate, i consigli e le videochiamate Bologna-Torino. Grazie per essermi rimasta vicina nonostante tutto. Se c'è una cosa che nessuno potrà mai cambiare è il bene che ci vogliamo.

Ringrazio le mie amiche, Elena e Juela. Custodisco gelosamente le nostre risate, le nostre uscite pre-ripartenza, il nostro viaggio, i nostri sguardi al futuro e tutte le emozioni che viviamo insieme ormai da vent'anni. Grazie per essere il porto sicuro in cui posso rifugiarmi sempre.

Ringrazio Marzia, la mia amica di sempre. Da quando eravamo bambine ogni discussione è sempre finita in un abbraccio. Non importa quanto il tempo ci abbia tenute distanti perchè se mi volto indietro sono certa di incrociare il tuo sguardo

sempre. Grazie a Beatrice. Come mi hai scritto una volta "un pretesto per tornare bisogna sempre seminarselo dietro quando si parte". Il mio pretesto sei stata tu. Grazie a tutti i miei amici di giù, Tania, Davide, Alessandro G., Maria, Alessandro T., Dario, Sara, Lorenzo. Grazie per non avermi mai fatto dimenticare quanto è bello il profumo di casa. Nel vostro piccolo siete riusciti ad essere la mia forza.

Grazie a tutto il team "Dario's fellas": siete stati la mia famiglia in questi mesi a Londra. Porterò sempre con me le risate, gli abbracci, gli insegnamenti, le tazze di caffè tra una poltrona e l'altra, i "lunch in 5". Ognuno di voi mi ha insegnato qualcosa. Siete stati voi la mia esperienza a Londra. Un grazie particolare va ai miei supervisor per scelta: Simone, Andrea e Andrea Stefano C. Grazie per il supporto di questi mesi, per avermi aiutata e spronata in questo progetto. Siete stati indispensabili.

Thank you Fah. You have been the most beautiful surprise that London could gave me. With you, I understood that you must always smile to life. Thank you for your "Nooo Mariaaannna", for letting me rediscover what simplicity is.

Il mio ultimo pezzo di nastro si riavvolge su Torino; sono certa che un pezzo di me ti apparterrà per sempre. A tutte le esperienze che ho vissuto in questa città, ad ogni persona che ho incontrato in questi anni. A chi c'è ancora, a chi ha scelto di non esserci più e di intraprendere un percoso che non si incrocia più con il mio. A chi è stato solo di passaggio ma mi ha lasciato un'enorme impronta dentro. Ad ogni risata che sento risuonare nelle aule e nei corridoi del Politecnico, ad ogni chiacchierata con i piedi a penzoloni in riva al Po. Alle corse di domanica mattina nel Parco Del Valentino, alle Desperados bevute a gambe incrociate in Piazza Santa Giulia, alla bicicletta rubata/comprata a Porta Palazzo. A casa AFF: in quelle mura sono nate due delle mie più grandi amicizie. Non importa dove voi siate, dove sarete e cosa siamo adesso, sappiate che mi avete cambiato la vita. Ringrazio in particolare i miei amici Anna, Alessandro Q., Stefano G., Andrea T., Stefano M., Erica, Alice, Stefania, Andrea V., Fabiano, Edoardo, MariaCarla, Giulia L., Francesca, Carla, Eva, Simone. Ognuno di voi mi ha cambiata e migliorata. Grazie ad Andrea P., compagno della mia avventura a Londra. Se oggi credo di più in me stessa è soprattutto merito delle tue cazziate.

A nonna Nice e nonno Peppino: non so esattamente dove voi siate in questo momento ma in questi anni ho imparato a dare una risposta a questa domanda "Perché dovrei essere fuori dai tuoi pensieri e dalla tua mente, solo perché sono fuori dalla tua vista?". Questo traguardo lo dedico a voi, alla vostra prima nipote laureata.

A nonno Giovanni. Ai tuoi "maccheroni con il sugo". Sono certa che sei ancora seduto nella tua punto azzurra con quel "pronti " che andiamo ovunque. Oggi brindiamo insieme con un bicchiere di vino rosso. Oggi non devi nasconderlo a nessuno. A nonna Maria: qualcosa mi fa pensare che la seconda corona d'alloro l'avresti voluta vedere anche tu.

Con il sorriso sul viso e la paura di quello che da domani sarà, voglio dire grazie

a me stessa. Se c'è una cosa che ho imparato in questi ultimi mesi è cercare di vedere il lato positivo in tutto, ad affrontare la vita con il sorriso perchè alla fine le soddisfazioni arrivano sempre. Nonostante le mie continue insicurezze, ansie e il non sentirmi mai all'altezza ho chiuso un secondo grande capitolo della mia vita. Sono felice e fiera di essere arrivata fin qui.